JCB Journal of Cell Biology

ARTICLE

PERK prevents rhodopsin degradation during retinitis pigmentosa by inhibiting IRE1-induced autophagy

Ning Zhao[1], Ning Li[2], and Tao Wang[1,2,3,4]

Chronic endoplasmic reticulum (ER) stress is the underlying cause of many degenerative diseases, including autosomal dominant retinitis pigmentosa (adRP). In adRP, mutant rhodopsins accumulate and cause ER stress. This destabilizes wild-type rhodopsin and triggers photoreceptor cell degeneration. To reveal the mechanisms by which these mutant rhodopsins exert their dominant-negative effects, we established an in vivo fluorescence reporter system to monitor mutant and wild-type rhodopsin in *Drosophila*. By performing a genome-wide genetic screen, we found that PERK signaling plays a key role in maintaining rhodopsin homeostasis by attenuating IRE1 activities. Degradation of wild-type rhodopsin is mediated by selective autophagy of ER, which is induced by uncontrolled IRE1/XBP1 signaling and insufficient proteasome activities. Moreover, upregulation of PERK signaling prevents autophagy and suppresses retinal degeneration in the adRP model. These findings establish a pathological role for autophagy in this neurodegenerative condition and indicate that promoting PERK activity could be used to treat ER stress-related neuropathies, including adRP.

Introduction

Defects in protein folding are a common cellular event, typically resulting from genetic mutations, translational errors, or a range of cellular stresses. Thus, maintaining an intact proteasome and cellular function requires continuous removal of misfolded proteins (Kurtishi et al., 2019). Eukaryotic cells are equipped with a number of physiological mechanisms to ensure proteins are correctly folded and to degrade misfolded proteins, but a prolonged imbalance between the generation of misfolded proteins and quality control mechanisms can disrupt cellular function. This underlies many diseases, including neurodegenerative disorders (Klaips et al., 2018). In eukaryotic cells, the ER is an intracellular organelle central to the synthesis of secretory and membrane proteins (Sano and Reed, 2013). When cells experience stress (e.g., oxidative stress or aging), the accumulation of misfolded proteins results in a loss of proteostasis. These misfolded proteins accumulate in the ER resulting in the activation of the unfolded protein response (UPR). The UPR is a cellular homeostatic mechanism that reduces ER stress by promoting the degradation of misfolded proteins and slowing the synthesis of new proteins (Hetz et al., 2020; Walter and Ron, 2011).

The UPR is controlled by three ER-resident transmembrane proteins, inositol-requiring enzyme 1 (IRE1), activating transcription factor 6 (ATF6), and protein kinase RNA-like ER kinase (PERK; Walter and Ron, 2011). Upon ER stress, PERK oligomerizes, leading to phosphorylation of eukaryotic initiation factor 2α (eIF2α). Phosphorylated eIF2α binds and inhibits the guanine nucleotide exchange factor, eIF2B, thereby attenuating eIF2-mediated protein synthesis (Adomavicius et al., 2019; Kenner et al., 2019). In contrast with the global repression of translation, eIF2α phosphorylation also activates the stress-responsive transcription factors, ATF4 and Xrp1, through selectively enhanced translation (Brown et al., 2021; Harding et al., 1999; Harding et al., 2003). Xrp1 is a newly discovered transcription factor induced downstream of PERK in *Drosophila* (Brown et al., 2021). In addition, UPR signaling activates the IRE1 nuclease, which targets and splices mRNA encoding the transcription factor X-box-binding protein 1 (XBP1), thereby activating it. Activated XBP1 then upregulates genes involved in ER protein folding, as well as genes promoting the degradation of misfolded proteins (Calfon et al., 2002; Cox et al., 1993; Haze et al., 1999; Yoshida et al., 2001). Transcriptional targets of XBP1 and ATF6 overlap significantly; the latter undergoes stress-induced intramembrane proteolytic processing and translocates to the nucleus (Mori et al., 1993; Shoulders et al., 2013). The

[1]Peking Union Medical College, Chinese Academy of Medical Sciences, Beijing, China; [2]College of Biological Sciences, China Agricultural University, Beijing, China; [3]Tsinghua Institute of Multidisciplinary Biomedical Research, Tsinghua University, Beijing, China; [4]National Institute of Biological Sciences, Beijing, China.

Correspondence to Tao Wang: wangtao1006@nibs.ac.cn.

three UPR pathways, in particular the IRE1 and PERK branches, have different activating states, and unequal or contradictory effects on cellular pathophysiology, depending on the disease and physiological context (Chang et al., 2018; Lin et al., 2007; Zhu et al., 2019). Consistent with their different activating states, the inhibition of translation by PERK attenuates IRE1 activation following a prolonged UPR state. However, the mechanisms by which one UPR branch affects another and the physiological significance of this regulation are not understood (Chang et al., 2018; Lin et al., 2007).

Autosomal dominant retinitis pigmentosa (adRP), the most common form of retinal degeneration, is most often caused by dominant mutations in the rhodopsin gene (*Rho*). Resulting mutant G protein-coupled receptors (GPCR) are misfolded and accumulate in the ER (Athanasiou et al., 2018; Hartong et al., 2006; Mendes et al., 2005). The substitution of proline 23 by histidine (RHO^{P23H}), the most common adRP-associated mutation, results in rhodopsin improper folding, retention in the ER, activation of the UPR, and ultimately photoreceptor degeneration (Dryja et al., 1990; Lin et al., 2007). Interestingly, this mutated opsin exerts a dominant negative effect on wild-type RHO, as co-expression of wild-type RHO and RHO^{P23H} results in: (1) mislocalized wild-type RHO, (2) formation of inclusions that contain wild-type RHO, and (3) enhanced proteasome-mediated degradation of wild-type RHO (Mendes and Cheetham, 2008; Rajan and Kopito, 2005; Saliba et al., 2002). In a Rho^{P23H} knock-in mouse model, levels of wild-type RHO are decreased, and heterozygous animals exhibit retinal degeneration in the rod outer segment (Sakami et al., 2011). Similarly, *Drosophila* carrying a heterozygous mutation in the major rhodopsin, Rh1 ($ninaE^{G69D}$), which is encoded by the *ninaE* locus, exhibits low levels of both mutated and wild-type Rh1 (Colley et al., 1995). Compounds that reduce the dominant-negative effects of the RHO^{P23H} opsin alleviate cell death, suggesting that the interruption of opsin homeostasis by dominant RHO is involved in adRP pathology (Mendes and Cheetham, 2008). Although it is clear that misfolded rhodopsin dominant negatively affects the wild-type protein, the mechanisms and physiological role have not been identified.

IRE1 and ATF6 can both upregulate the expression of chaperones involved in RHO folding, as well as ER-associated degradation (ERAD) components that specifically remove and degrade misfolded proteins via the ubiquitin–proteasome system (UPS), thereby leading to the degradation of misfolded RHO while sparing the wild-type version (Chiang et al., 2015; Chiang et al., 2012b; Lin et al., 2007; Ryoo et al., 2007; Shoulders et al., 2013). In addition to ERAD, the autophagy pathway, which is a second cellular quality control mechanism for clearing damaged proteins, is actively involved in regulating turnover of ER proteins and the ER itself (Khaminets et al., 2015). Induction of autophagy is observed in Rho^{P23H} mice, leading to proteasome insufficiency and increased retinal degeneration (Qiu et al., 2019; Yao et al., 2018). It has been suggested that the levels of autophagy increase as a result of the loss of *Atf6* (Lee et al., 2021). Recently in a *Drosophila* model of Parkinson's disease, overexpression of IRE1 was shown to induce autophagy and triggers neuronal cell death in an XBP1-independent manner (Yan et al., 2019). By contrast to the selective reduction of mutant opsin through ATF6 or IRE1 signaling, the PERK pathway shows no such specificity, reducing both wild-type and mutant RHO protein levels. This suggests that PERK is involved in the non-selectively removal of ER proteins (Chiang et al., 2012a). It remains unclear how the UPR induces autophagy, and whether the selective autophagy of ER is responsible for maintaining cellular protein homeostasis.

In the present study, we established an in vivo model in *Drosophila* to study the dominant effects of misfolded rhodopsin on the wild-type protein. In this model, we changed proline 37 to histidine ($Rh1^{P37H}$ is equivalent to mammalian RHO^{P23H}) and tagged this mutant opsin with GFP. We also tagged wild-type Rh1 with RFP and co-expressed these proteins in photoreceptor cells (Galy et al., 2005; Griciuc et al., 2010). Using this newly developed system, we conducted a forward genetic screen to identify genes that enhance the dominant effects of $Rh1^{P37H}$. We found that the PERK pathway played a key role in maintaining levels of wild-type Rh1 and in sustaining photoreceptor cell function and integrity in $Rh1^{P37H}$-expressing cells. This effect was independent of ATF4. In animals lacking the PERK pathway, IRE1/XBP1 signaling was over-activated, leading to massive autophagy and degradation of wild-type rhodopsin. Finally, in a fly model of adRP, induction of PERK signaling prevented the induction of autophagy and thus suppressed retinal degeneration.

Results

Rhodopsin homeostasis is disrupted by mutations in *perk* and *eIF2Bα* in a dominant Rh1 mutant fly model

To study the genetic interactions between misfolded and wild-type versions of rhodopsin in vivo, we modified the previously established *Drosophila* model of adRP by co-expressing GFP-tagged $Rh1^{P37H}$ and RFP-tagged wild-type Rh1 using the endogenous *ninaE* promotor (*ninaE, neither inactivation nor afterpotential E*; Fig. 1 A; Galy et al., 2005; Griciuc et al., 2010; O'Tousa et al., 1985; Zuker et al., 1985). Consistent with previous reports, $Rh1^{P37H}$-GFP accumulated exclusively in the ER, co-localizing with the ER marker CNX (calnexin). By contrast, wild-type Rh1-RFP localized to the rhabdomeres with endogenous Rh1 and INAD (Fig. 1 D; Galy et al., 2005). Moreover, $Rh1^{P37H}$-GFP induced ER stress, as both ATF4-mCherry and XBP1-mCherry (two independent reporters of ER stress) were expressed and activated in $Rh1^{P37H}$*-GFP* retinas, but not in retinas expressing wild-type Rh1-GFP (Kang and Ryoo, 2009; Xu et al., 2020; Fig. 1, E–H). Importantly, expression of misfolded $Rh1^{P37H}$-GFP resulted in less wild-type Rh1 but did not affect levels of endogenous TRP and INAD. This indicates that disease-causing rhodopsin mutations mildly impaired rhodopsin homeostasis (Fig. 1, B and C).

Combining this $Rh1^{P37H}$-GFP/Rh1-RFP reporters with the "*ey-flp/hid*" system, which generates flies in which EMS-induced mutations are homozygous in the eye but heterozygous in the rest of the animal, we performed EMS mutagenesis and screened chromosomes 2 and 3 (including 2L, 2R, 3L, and 3R) for mutants in which $Rh1^{P37H}$-GFP further disrupted the homeostasis of wild-type Rh1 (Fig. S1 A; Xiong et al., 2020; Zhao et al., 2018). For each

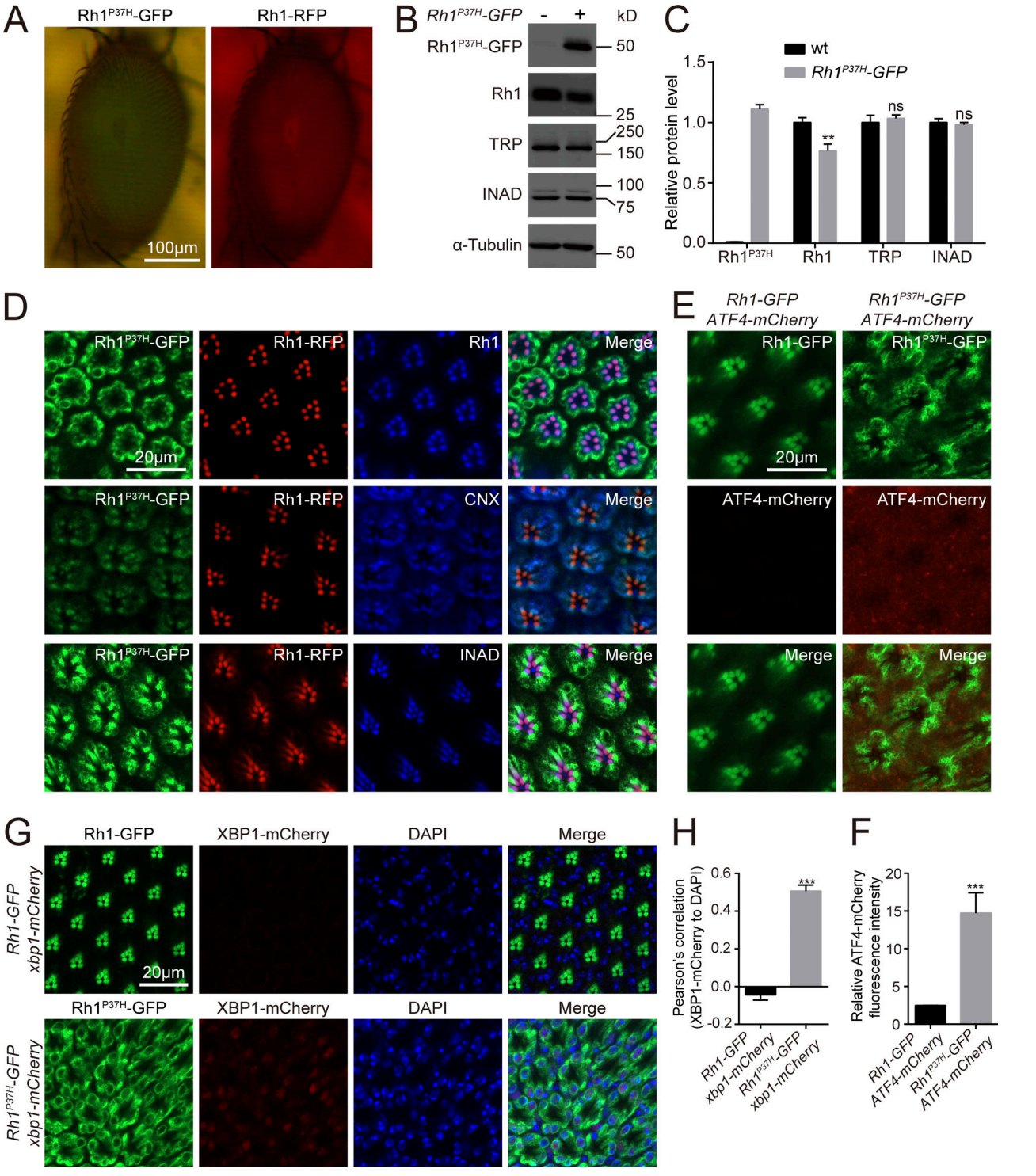

Figure 1. **Establishment of a Rh1^{P37H}-GFP-based *Drosophila* model of autosomal dominant retinitis pigmentosa (adRP). (A)** Representative images of compound eyes expressing Rh1^{P37H}-GFP and Rh1-RFP. Scale bar, 100 μm. **(B)** Western blot revealed that expression of Rh1^{P37H}-GFP reduced the endogenous protein levels of wild-type Rh1. Anti-Rh1 antibodies failed to recognize c-terminal tagged Rh1 (Rh1-GFP/RFP). 1-d-old flies raised under 12-h-light–12-h-dark cycles were used. α-tubulin was used as a loading control. **(C)** Quantification of relative levels of endogenous Rh1, TRP, and INAD from B. Error bars indicate SEM (n = 3); ns, not significant; **P < 0.01 (two-way ANOVA, Sidak's multiple comparisons test). **(D)** Tangential views of retina from ∼1-d-old *Rh1-RFP*; *Rh1^{P37H}-GFP* flies labeled using anti-Rh1, anti-CNX (calnexin), and anti-INAD antibodies (blue). GFP fluorescence of Rh1^{P37H}-GFP (green) and RFP fluorescence of Rh1-RFP (red) were directly observed. Scale bar, 20 μm. **(E)** Retinas of adult *Rh1-GFP* and *Rh1^{P37H}-GFP* flies expressing *ATF4-mCherry*.1-d-old flies raised under 12-h-light–12-h-dark cycles were used. Scale bar, 20 μm. **(F)** Quantification of relative mCherry fluorescence intensity showed that the ER stress reporter ATF4-mCherry (E) was activated by Rh1^{P37H}-GFP but not by wild-type Rh1-GFP. Error bars indicate SEM (n = 3); ***P < 0.001 (Student's unpaired t test). **(G)** Retinas of adult *Rh1-GFP* and *Rh1^{P37H}-GFP* flies expressing *xbp1-mCherry*. 1-d-old flies raised under 12-h-light–12-h-dark cycles were used. Scale bar, 20 μm. **(H)** Quantification of the co-localization between XBP1-mCherry and DAPI in flies that express Rh1-GFP or Rh1^{P37H}-GFP. Error bars indicate SEM (n = 3); ***P < 0.001 (Student's unpaired t test). Source data are available for this figure: SourceData F1.

chromosome arm we screened ~100,000 flies, isolating 4 alleles in which RFP but not GFP fluorescence was reduced. These four alleles belonged to two complementation groups, both located on the right arm of chromosome 3 (3R). Using deficiency mapping and genomic DNA sequencing, we found that one complementation group localized to the *perk* locus ($perk^{l2}$, $perk^{34}$, $perk^{46}$), and the other localized to the *eIF2Bα* gene ($eIF2B\alpha^{39}$; Fig. 2, A and B). These four alleles contain single-nucleotide changes within the coding region causing missense mutations in PERK and eIF2Bα proteins (Fig. S1, B–E). Flies heterozygous for any of these *perk* or *eIF2Bα* alleles did not exhibit a phenotype, regardless of whether they express $Rh1^{P37H}$-GFP or not, suggesting that these are loss of function mutations. We confirmed via Western blotting that levels of endogenous wild-type Rh1 were greatly reduced in $perk^{l2}$ and $eIF2B\alpha^{39}$ mutant animals, whereas $Rh1^{P37H}$-GFP accumulated (Fig. 2 C and Fig. S1 F). Importantly, the lower MW $Rh1^{P37H}$-GFP bands in $perk^{l2}$ and $eIF2B\alpha^{39}$ mutant extracts are non-glycosylated versions of the protein, suggesting that ER function was impaired. Moreover, expression of wild-type PERK or eIF2Bα in $perk^{l2}$ or $eIF2B\alpha^{39}$ mutants, respectively, restored levels of endogenous Rh1 and reduced levels of $Rh1^{P37H}$-GFP to control levels (Fig. 2 C and Fig. S1 F).

During biosynthesis, Rh1 is transiently glycosylated in the ER. This modification is gradually removed as Rh1 is transported from the ER to the rhabdomere (Rosenbaum et al., 2014). A band of Rh1 with an increased molecular weight (MW) was observed in $Rh1^{P37H}$-*GFP* $perk^{l2}$ and $Rh1^{P37H}$-*GFP* $eIF2B\alpha^{39}$ mutant flies, indicating a defective maturation process for wild-type rhodopsin (Fig. 2 C). We then examined the localization of wild-type Rh1 and $Rh1^{P37H}$-GFP in $perk^{l2}$ and $eIF2B\alpha^{39}$ mutants. In these mutant retinas, both wild-type Rh1-RFP and endogenous Rh1 colocalized with $Rh1^{P37H}$-GFP in the ER, whereas INAD still localized to the rhabdomeres. This indicates that trafficking of wild-type Rh1 was disrupted by *perk* and *eIF2Bα* mutations with misfolded $Rh1^{P37H}$ expression (Fig. 2 E and Fig. S1 G). We next asked if mutations in *perk* and *eIF2Bα* affected the biosynthesis and trafficking of rhodopsin. We found that Rh1 levels and localization were normal in both $perk^{l2}$ and $eIF2B\alpha^{39}$ mutant photoreceptor cells (without $Rh1^{P37H}$ expression; Fig. 2, D and E). These results indicate that PERK and eIF2Bα help maintain the homeostasis of wild-type rhodopsin when misfolded form is present.

Since Rh1 is essential for photoreceptor function, we asked whether phototransduction was disrupted in *perk* and *eIF2Bα* mutants. ERG (electroretinogram) recordings measure the summed light responses of all retinal cells. In flies with normal levels of functional rhodopsin, a prolonged depolarization afterpotential (PDA) is induced upon exposure to blue light (Fig. 2 F; Wang and Montell, 2007). Flies expressing $Rh1^{P37H}$ exhibited a normal PDA, consistent with a slight reduction in wild-type Rh1 levels. However, no PDAs were detected in $perk^{l2}$ and $eIF2B\alpha^{39}$ mutants expressing $Rh1^{P37H}$, consistent with the large reduction in wild-type Rh1 levels (Fig. 2 F). In contrast, $perk^{l2}$ and $eIF2B\alpha^{39}$ mutants that lacked $Rh1^{P37H}$ expression exhibited normal PDAs when exposed to blue light (Fig. 2 F). As disruptions in rhodopsin homeostasis are associated with the progression of retinal degeneration in adRP diseases, we next asked if disrupting PERK and eIF2Bα aggravates the severity of retinal degeneration in the $Rh1^{P37H}$-*GFP* model. We used TEM to first assess young (1-d-old) and aged (10-d-old) wild-type, $Rh1^{P37H}$-*GFP*, $perk^{l2}$, and $eIF2B\alpha^{39}$ flies. For each age and genotype, seven intact rhabdomeres were consistently detected in each ommatidia (Fig. 2 G). In the $Rh1^{P37H}$-*GFP* background, young $perk^{l2}$ and $eIF2B\alpha^{39}$ mutants exhibited normal retinal morphology with all 7 rhabdomeres, although the rhabdomeres were smaller. However, aged flies of these genotypes ($perk^{l2}$ or $eIF2B\alpha^{39}$ mutations in the $Rh1^{P37H}$-*GFP* background) exhibited severe retinal degeneration with prominent vacuoles and loss of rhabdomeres (Fig. 2 G). Therefore, we conclude that PERK and eIF2Bα are required for photoreceptor survival in the context of $Rh1^{P37H}$-induced ER stress.

The PERK pathway is the major UPR axis maintaining rhodopsin homeostasis independent of ATF4

Misfolded rhodopsin causes ER stress and activates three UPR pathways, namely, the PERK, IRE1, and ATF6 pathways (Harding et al., 2000b; Liu et al., 2000; Shamu and Walter, 1996; Shen et al., 2002). Once activated, PERK phosphorylates eIF2α and promotes its inhibitory binding to the nucleotide exchange factor eIF2B to regulate translation initiation. Therefore, mutations in either the *perk* or *eIF2Bα* genes would impair the PERK/eIF2α branch of the UPR response. Since our screen did not identify genes involved in the IRE1 or ATF6 pathways, we hypothesized that the PERK/eIF2α axis is the major UPR branch involved in maintaining rhodopsin homeostasis under ER stress. To test this hypothesis, we first generated a null allele of *atf6* ($atf6^{1}$) using the CRISPR/CAS9 technique (Fig. S2, C and D). Resulting mutants were viable. A loss of function mutation for the *ire1* gene ($ire1^{f02170}$) was already available (Coelho et al., 2013). Unlike we saw for the *perk* mutant, levels of $Rh1^{P37H}$ and endogenous Rh1 were unaffected in homozygous $ire1^{f02170}$ or $atf6^{1}$ mutants compared with $Rh1^{P37H}$-*GFP* flies (Fig. S2, E–H).

To further demonstrate that the PERK/eIF2α pathway is the major UPR axis regulating rhodopsin homeostasis in the $Rh1^{P37H}$ model, we expressed $eIF2\alpha^{S51A}$ to abolish PERK-dependent eIF2α phosphorylation. Consistent with data from the $perk^{l2}$ and $eIF2B\alpha^{39}$ mutants, expression of $eIF2\alpha^{S51A}$ led to the accumulation of $Rh1^{P37H}$-GFP and reduction of endogenous Rh1 (Fig. 3, A and B). Phosphorylated eIF2α inhibits the translation of most proteins, but selectively activates translation of the transcription factor ATF4 (Fawcett et al., 1999; Harding et al., 2000a). As we have previously shown, ATF4 expression is induced in the $Rh1^{P37H}$ model (Fig. 1, E and F). We then tested whether induction of ATF4 is involved in the regulation of rhodopsin homeostasis. We first generated a null allele of *atf4* ($atf4^{KO}$) by deleting a 462 base pair fragment using CRISPR/CAS9 (Fig. S2, A and B). However, knocking out *atf4* did not result in the accumulation of $Rh1^{P37H}$-GFP or reduced levels of endogenous Rh1 (Fig. 3, C and D). Moreover, continuous expression of ATF4 without its translational regulation sequence under a ubiquitously expressed *da* (*daughterless*) promotor failed to rescue the accumulation of $Rh1^{P37H}$-GFP and reduction of Rh1 caused by loss of *perk* (Fig. 3, E and F). These data demonstrated that the PERK/eIF2 pathway regulates homeostasis of rhodopsin under chronic ER stress independent of ATF4.

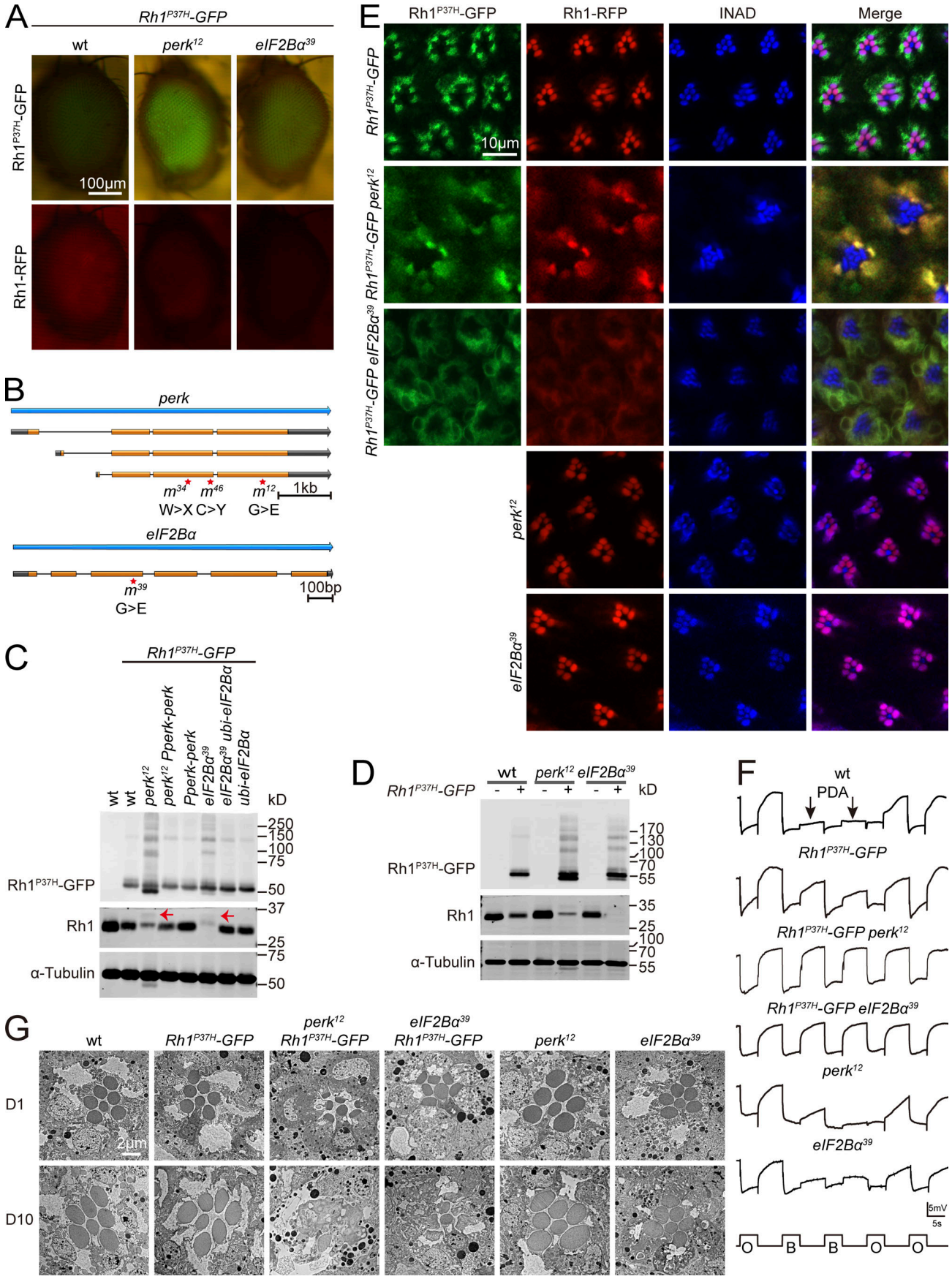
A
Rh1P37H-GFP
wt
perk12
eIF2Bα39
Rh1P37H-GFP
Rh1-RFP
100μm
B
perk
m34 m46 m12
W>X C>Y G>E
1kb
eIF2Bα
m39
G>E
100bp
C
Rh1P37H-GFP
wt
wt
perk12
perk12 Pperk-perk
Pperk-perk
eIF2Bα39
eIF2Bα39 ubi-eIF2Bα
ubi-eIF2Bα
kD
Rh1P37H-GFP
Rh1
α-Tubulin
250
150
100
75
50
37
25
75
50
D
Rh1P37H-GFP
wt
perk12
eIF2Bα39
- + - + - +
kD
Rh1P37H-GFP
Rh1
α-Tubulin
170
130
100
70
55
35
25
100
70
55
E
Rh1P37H-GFP
Rh1-RFP
INAD
Merge
Rh1P37H-GFP
10μm
Rh1P37H-GFP perk12
Rh1P37H-GFP eIF2Bα39
perk12
eIF2Bα39
F
wt
PDA
Rh1P37H-GFP
Rh1P37H-GFP perk12
Rh1P37H-GFP eIF2Bα39
perk12
eIF2Bα39
5mV
5s
O B B O O
G
wt
Rh1P37H-GFP
perk12 Rh1P37H-GFP
eIF2Bα39 Rh1P37H-GFP
perk12
eIF2Bα39
D1
D10
2μm

Figure 2. **Rhodopsin homeostasis is disrupted by mutations in *perk* or *eIF2Bα* in the adRP model. (A)** Isolation of $perk^{12}$ and $eIF2B\alpha^{39}$ mutants via a forward genetic screen. Rh1-RFP and $Rh1^{P37H}$–GFP fluorescence were detected using a Stereo Fluorescence Microscope. Images from wild-type (*ey-flp Rh1-RFP; $Rh1^{P37H}$-GFP*), $perk^{12}$ (*ey-flp Rh1-RFP; FRT82B $Rh1^{P37H}$-GFP $perk^{12}$/FRT82B GMR-hid CL*), and $eIF2B\alpha^{39}$ (*ey-flp Rh1-RFP; FRT82B $Rh1^{P37H}$-GFP $eIF2B\alpha^{39}$/FRT82B GMR-hid CL*) flies are shown. Scale bar, 100 µm. **(B)** The *perk* and *eIF2Bα* loci and mutations associated with the $perk^{12}$, $perk^{34}$, $perk^{46}$, and $eIF2B\alpha^{39}$ alleles. **(C)** Western blot of heads dissected from wild-type, $perk^{12}$, and $eIF2B\alpha^{39}$ flies expressing $Rh1^{P37H}$-GFP. Levels of GFP and Rh1 are shown. Expressing PERK via the endogenous *perk* promoter (*Pperk-perk*) and eIF2Bα under a *ubiquitin* promoter (*ubi-eIF2Bα*) rescued the phenotypes. 1-d-old flies were used, and α-tubulin was used as a loading control. Bands of Rh1 with increased molecular weight (MW) in $Rh1^{P37H}$-GFP $perk^{12}$ and $Rh1^{P37H}$-GFP $eIF2B\alpha^{39}$ mutant flies are indicated by red arrows. **(D)** Western blot analysis of Rh1 in homozygous $perk^{12}$ (*ey-flp Rh1-RFP; FRT82B $perk^{12}$/FRT82B GMR-hid CL*) and $eIF2B\alpha^{39}$ (*ey-flp Rh1-RFP; FRT82B $eIF2B\alpha^{39}$/FRT82B GMR-hid CL*) mutants without $Rh1^{P37H}$ expression. **(E)** Tangential views of wild-type, $perk^{12}$, and $eIF2B\alpha^{39}$ retina expressing $Rh1^{P37H}$-GFP and Rh1-RFP or homozygous $perk^{12}$ (*ey-flp Rh1-RFP; FRT82B $perk^{12}$/FRT82B GMR-hid CL*) and $eIF2B\alpha^{39}$ (*ey-flp Rh1-RFP; FRT82B $eIF2B\alpha^{39}$/FRT82B GMR-hid CL*) mutants without $Rh1^{P37H}$ expression labeled for INAD (blue, a rhabdomere marker). GFP fluorescence of $Rh1^{P37H}$-GFP (green) and RFP fluorescence of Rh1-RFP (red) were directly observed. Scale bar, 10 µm. **(F)** ERG recordings of wt (*Rh1-GFP*) and $Rh1^{P37H}$-GFP (*ey-flp Rh1-RFP; $Rh1^{P37H}$-GFP*) flies showed that a PDA was induced by blue light (arrows). The PDA was eliminated in $perk^{12}$ (*ey-flp Rh1-RFP; FRT82B $Rh1^{P37H}$-GFP $perk^{12}$/FRT82B GMR-hid CL*), and $eIF2B\alpha^{39}$ (*ey-flp Rh1-RFP; FRT82B $Rh1^{P37H}$-GFP $eIF2B\alpha^{39}$/FRT82B GMR-hid CL*) flies. ERG recordings of $perk^{12}$ and $eIF2B\alpha^{39}$ mutants without $Rh1^{P37H}$ expression showed normal PDAs. 1-d-old flies were exposed to 5-s pulses of orange (O) or blue (B) light as indicated. At least 10 flies of each genotype were tested. **(G)** TEM images of eye tangential sections from 1-d-old and 10-d-old flies. Genotypes are indicated. Scale bar, 2 µm. All flies were in white eye background and raised under 12 h light/12 h dark cycles. Source data are available for this figure: SourceData F2.

Over-activation of the IRE1/XBP1 axis is involved in reducing wild-type Rh1

To identify factors that act downstream of PERK/eIF2α to help maintain rhodopsin homeostasis, we performed an RNA-seq analysis to identify genes that are up- or down-regulated in *perk* mutants. As with the $perk^{12}$ mutant, knocking down *perk* by RNAi reduced endogenous Rh1 levels and increased levels of $Rh1^{P37H}$-GFP, although to a lesser extent (Fig. 4 E). By contrast, expressing $perk^{RNAi}$ in a wild-type Rh1 background did not affect Rh1 homeostasis. We therefore compared the transcriptomes of $Rh1^{P37H}$-GFP $perk^{RNAi}$ and $Rh1^{P37H}$-GFP flies (Fig. 4 A). Most genes that were strongly upregulated by expression of $perk^{RNAi}$ were targets of the IRE1/XBP1 pathway (Hollien and Weissman, 2006). To confirm this, we used RNA-seq to identify genes upregulated by spliced XBP1. We generated *ninaE-xbp1-RE* flies in which the RE form of *xbp1* (the version of *xbp1* that has been spliced by IRE1) is expressed in photoreceptor cells using the *ninaE* promotor. Importantly, most genes that were upregulated in *perk* mutant retinas were also induced by *ninaE-xbp1-RE* (Fig. S3, A and B). To further validate the RNA-seq results, we used RT-qPCR to confirm that the major IRE1/XBP1-induced genes (including *Hsc70-3*, *CaBP1*, *BI-1*, *Gp93*, *Ero1L*, and *Sec22*) were upregulated in the $Rh1^{P37H}$-GFP $perk^{RNAi}$ retina. Importantly, upregulation of these genes was completely reversed by knocking down *ire1* using $ire1^{RNAi}$, further suggesting that the IRE1/XBP1 axis is activated when the PERK/eIF2α pathway is blocked during ER stress (Fig. 4 B). Since total *xbp1* mRNA levels were unaffected by $perk^{RNAi}$ (Fig. 4 C), we next asked whether the splicing of *xbp1* mRNA by IRE1 was induced upon loss of *perk*. We used qPCR to quantify the spliced (*sxbp1*) and unspliced (*uxbp1*) forms of *xbp1*. The ratio of *sxbp1/uxbp1* was slightly increased in $Rh1^{P37H}$-GFP flies, reflecting the mild induction of ER stress. By contrast, the *sxbp1/uxbp1* ratio dramatically increased in $Rh1^{P37H}$-GFP $perk^{RNAi}$ flies. This increase was totally abolished by $ire1^{RNAi}$, further confirming that IRE1 is strongly activated when PERK is blocked during $Rh1^{P37H}$-induced ER stress (Fig. 4 D).

PERK/eIF2α signaling generally inhibits translation, but it preferentially induces the translation of ATF4 during the UPR response. Given that the PERK/eIF2α pathway regulates rhodopsin homeostasis independent of ATF4, we speculated that PERK may negatively regulate IRE1 activity by inhibiting translation. To test this hypothesis, we re-inhibited translation in $Rh1^{P37H}$-GFP $perk^{RNAi}$ flies by knocking down the eukaryotic translation initiation factors *eIF3b* and *eIF4G*. We found that the *sxbp1/uxbp1* ratio decreased to wild-type levels (Fig. 4 D).

Since IRE1 is strongly activated in *perk* mutants upon ER stress, we next examined whether inhibition of the IRE1/XBP1 pathway contributes to rhodopsin homeostasis. We first knocked down *ire1* or *xbp1* in the background of $Rh1^{P37H}$-GFP $perk^{RNAi}$ and found that the levels of endogenous Rh1 were increased compared with control. However, the increase of $Rh1^{P37H}$-GFP in $perk^{RNAi}$ mutants was not alleviated, and even slightly aggravated by knocking down *ire1* or *xbp1* (Fig. 4, E and F). These data indicate that accumulation of mutant Rh1 and reduction of wild-type proteins are independent events regulated by different signaling pathways; the latter is mediated by IRE1/XBP1. Supporting this point, as seen when *ire1* or *xbp1* were knocked down, expressing $eIF3b^{RNAi}$ or $eIF4G^{RNAi}$ in the background of $Rh1^{P37H}$-GFP $perk^{RNAi}$ restored levels of wild-type Rh1 (Fig. 4, G and H). In contrast to *ire1* and *xbp1* knock down, when knocking down *eIF3b* or *eIF4G*, levels of $Rh1^{P37H}$-GFP in $Rh1^{P37H}$-GFP $perk^{RNAi}$ flies was also reduced to wild-type levels, supporting the hypothesis that reductions in translation efficiency by PERK activation is the major event involved in rhodopsin homeostasis (Fig. 4, G and H). As knocking down *ire1* or *xbp1* specifically prevented the loss of wild-type rhodopsin, we were able to examine if the loss of wild-type rhodopsin contributed to the retinal degeneration seen in $Rh1^{P37H}$-GFP $perk^{RNAi}$ flies. 5-d-old $Rh1^{P37H}$-GFP $perk^{RNAi}$ flies exhibited phenotypes associated with severe retinal degeneration, including reduced ERG responses and loss of rhabdomeres (Fig. S3, C–E). Expression of $xbp1^{RNAi}$ ameliorated ERG responses and suppressed the loss of photoreceptor cells in $Rh1^{P37H}$-GFP $perk^{RNAi}$ flies (Fig. S3, C–E). Considering that knocking down *ire1* or *xbp1* in the background of $Rh1^{P37H}$-GFP $perk^{RNAi}$ only alleviated reduction of wild-type Rh1 without affecting $Rh1^{P37H}$-GFP, loss of wild-type rhodopsin may be involved in the pathogenesis of this dominant rhodopsin disorder.

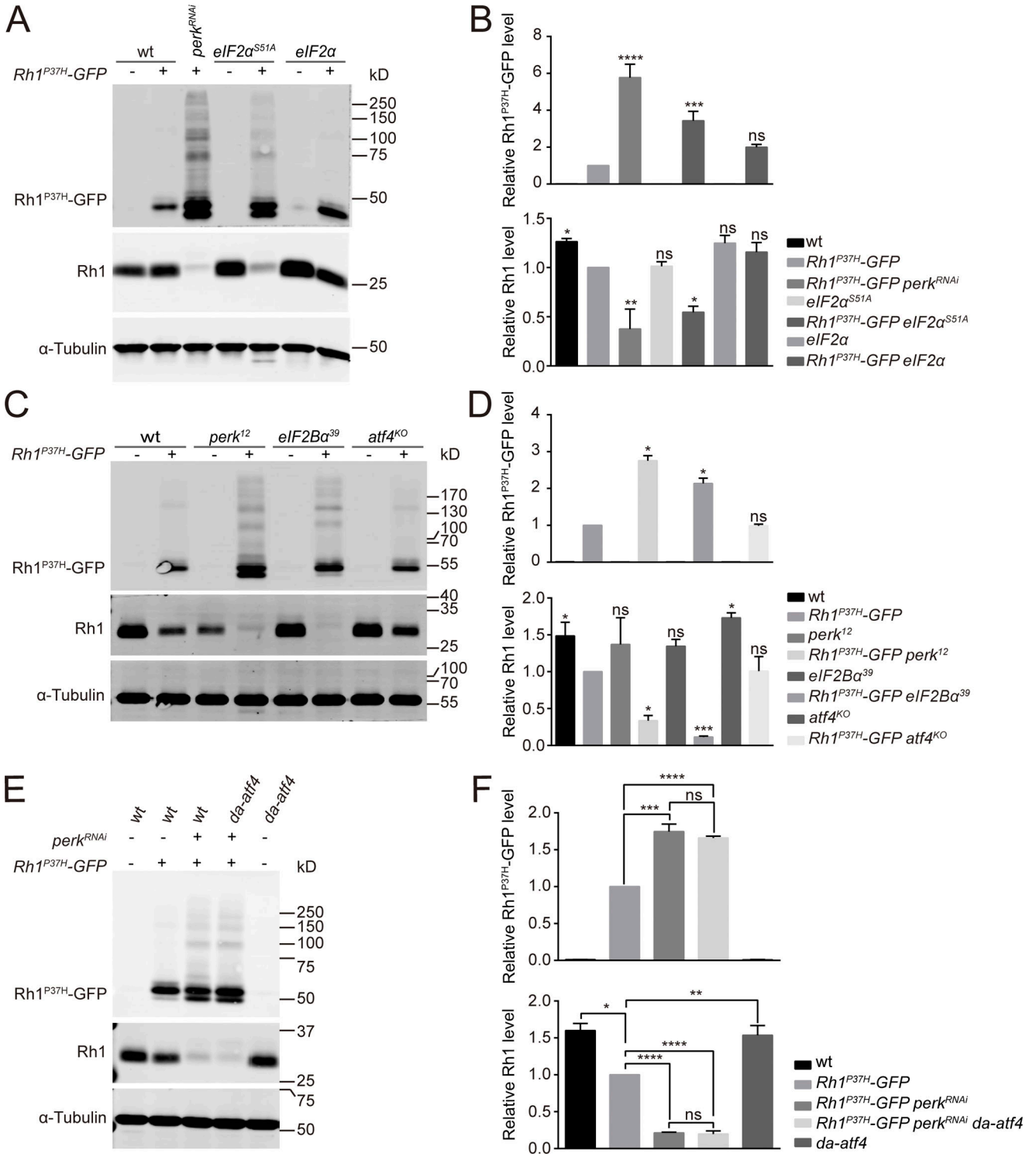

Figure 3. **The PERK/eIF2α signaling pathway maintains Rh1 homeostasis independent of ATF4. (A)** Western blot analysis of Rh1^{P37H}-GFP and endogenous Rh1 in *eIF2α^{S51A}* (*GMR-Gal4/UAS-eIF2α^{S51A} Rh1^{P37H}-GFP*) and *eIF2α* (*GMR-Gal4/UAS-eIF2α Rh1^{P37H}-GFP*) heads. Flies with *perk^{RNAi}* expression (*GMR-Gal4/UAS-perk^{RNAi} Rh1^{P37H}-GFP*) were used as a positive control. **(B)** Quantification of Rh1^{P37H}-GFP and endogenous Rh1 levels. Error bars indicate SEM (n = 3); ns, not significant, *P < 0.1, **P < 0.01, ***P < 0.001, ****P < 0.0001 (one-way ANOVA, Sidak's multiple comparisons test). **(C and D)** Western blot showed that levels of both Rh1^{P37H}-GFP and endogenous Rh1 were unchanged in *atf4^{KO}* (*atf4^{KO}; Rh1^{P37H}-GFP*) mutant flies, compared with wild-type control (*Rh1^{P37H}-GFP*). The *perk^{12}* and *eIF2Bα^{39}* flies were used as positive controls. Error bars indicate SEM (n = 3); ns, not significant, *P < 0.1, ***P < 0.001 (one-way ANOVA, Sidak's multiple comparisons test). **(E and F)** Western blot analysis showed that continuous expression of ATF4 failed to restore Rh1 homeostasis in *perk* knocked down flies. Levels of Rh1^{P37H}-GFP and wild-type Rh1 were examined (E) and quantified (F) in *perk* knocked down flies (*GMR-Gal4/UAS-perk^{RNAi} Rh1^{P37H}-GFP*) that expressed *atf4* (*da-atf4*). Error bars indicate SEM (n = 3); ns, not significant, *P < 0.1, **P < 0.01, ***P < 0.001, ****P < 0.0001 (one-way ANOVA, Sidak's multiple comparisons test). Source data are available for this figure: SourceData F3.

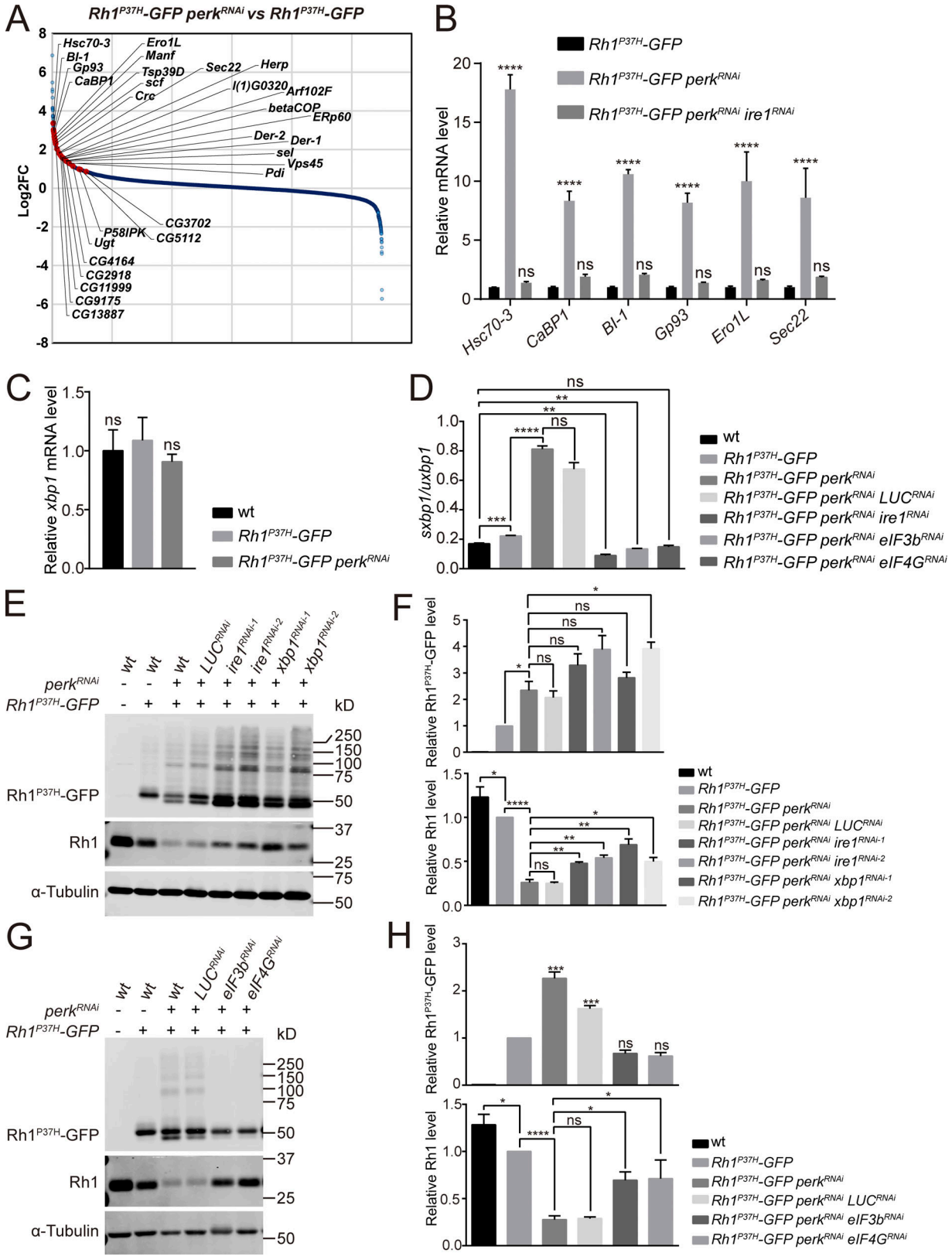

Figure 4. **Activation of the IRE1/XBP1 axis is involved in degrading wild-type Rh1. (A)** Transcriptome comparisons between retinas of *Rh1^{P37H}-GFP perk^{RNAi}* (*GMR-Gal4/UAS-perk^{RNAi} Rh1^{P37H}-GFP*) and *Rh1^{P37H}-GFP* flies. The genes strongly upregulated by spliced XBP1 are indicated by red dots. **(B)** qPCR analysis of *Hsc70-3*, *CaBP1*, *Bl-1*, *Gp93*, *Ero1L*, and *Sec22* to confirm the RNA-seq results. Error bars indicate SEM (n = 3); ns, not significant, ****P < 0.0001 (two-way ANOVA, Sidak's multiple comparisons test). The mRNAs were prepared from dissected retina of young (~1-d-old) flies with indicated genotypes. **(C)** qPCR analysis of the total mRNA levels of *xbp1* in wt, *Rh1^{P37H}-GFP*, and *Rh1^{P37H}-GFP perk^{RNAi}* retina. Error bars indicate SEM (n = 3); ns, not significant (one-way

ANOVA, Sidak's multiple comparisons test). **(D)** The *sxbp1* (spliced form)/*uxbp1* (unspliced form) ratio quantified from qPCR analysis. The mRNAs were prepared from dissected retina of ∼1-d-old flies with indicated genotypes. Error bars indicate SEM (n = 3); ns, not significant, **P < 0.01, ***P < 0.001, ****P < 0.0001 (one-way ANOVA, Sidak's multiple comparisons test). **(E and F)** Western blot analysis of $Rh1^{P37H}$-GFP and endogenous Rh1 showed that expressing $ire1^{RNAi}$ or $xbp1^{RNAi}$ significantly blocked the reduction of wild-type Rh1 by knocking down *perk* in $Rh1^{P37H}$-*GFP* models. Two independent $ire1^{RNAi}$ and $xbp1^{RNAi}$ lines were used, and LUC^{RNAi} was used as a control. Error bars indicate SEM (n = 3); ns, not significant, *P < 0.1, **P < 0.01, ****P < 0.0001 (one-way ANOVA, Sidak's multiple comparisons test). **(G and H)** Western blot analysis of $Rh1^{P37H}$-GFP and endogenous Rh1 showed that blocking translation by $eIF3b^{RNAi}$ and $eIF4G^{RNAi}$ suppressed both accumulation of $Rh1^{P37H}$-GFP and reduction of wild-type Rh1 in $Rh1^{P37H}$-*GFP* $perk^{RNAi}$ flies. LUC^{RNAi} was used as a negative control, and α-tubulin was used as a loading control. Error bars indicate SEM (n = 3); ns, not significant, *P < 0.1, ***P < 0.001, ****P < 0.0001 (one-way ANOVA, Sidak's multiple comparisons test). Source data are available for this figure: SourceData F4.

The selective autophagy of ER is involved in degradation of wild-type Rh1

Downregulation of wild-type Rh1 by the IRE1/XBP1 signaling pathway leads to the loss of rhodopsin homeostasis in $Rh1^{P37H}$ expressing cells. To investigate the mechanisms of this process, we used Tandem Mass Tag (TMT)–LC MS/MS to compare individual protein levels between $Rh1^{P37H}$-*GFP* $perk^{RNAi}$ and $Rh1^{P37H}$-*GFP* retinas. We identified 14 proteins that were greatly upregulated (P value <0.01) when *perk* was knocked down (Fig. 5 A). We then screened these 14 candidate genes by knocking them down in photoreceptor cells of $Rh1^{P37H}$-*GFP* $perk^{RNAi}$ flies. Only one gene, *ref(2)P/p62*, blocked the reduction of Rh1 when knocked down (Fig. 6, E and F). The *ref(2)P/p62* gene encodes an evolutionary conserved autophagy adaptor in *Drosophila*, indicating that autophagy is modulated in this context. We first verified that the Ref(2)P/P62 protein was upregulated in $Rh1^{P37H}$-*GFP* $perk^{RNAi}$ mutant retina by Western blotting and immunostaining. Importantly, this increase in Ref(2)P/P62 proteins was abolished by expressing $ire1^{RNAi}$ or $xbp1^{RNAi}$ (Fig. 5, B–D). Moreover, *ref(2)P/p62* mRNA levels were also elevated in $Rh1^{P37H}$-*GFP* $perk^{RNAi}$ flies; this could also be reversed by $ire1^{RNAi}$ (Fig. 5 E). These data indicated that the autophagy pathway may be induced by blocking the PERK pathway in $Rh1^{P37H}$ expressing photoreceptor cells. Consistent with this hypothesis, mRNA levels of several autophagy genes including *atg1*, *atg2*, *atg3*, *atg8a*, *atg9*, and *atg18a*, were also increased by $perk^{RNAi}$ in the context of $Rh1^{P37H}$-induced ER stress. Knocking down *ire1* suppressed these inductions (Fig. 5 F). We further measured levels of *hrd1* and *sordd1* mRNA, which encode two ER-associated ubiquitin ligases, and found that IRE1/XBP1 signaling also induced the expression of *hrd1* but not *sordd1* (Fig. 5 G).

To further confirm that autophagy is induced by loss of *perk* in $Rh1^{P37H}$-expressing photoreceptor cells, we labeled retinas for the autophagy marker, Atg8a, and Ref(2)P/P62. Both proteins accumulated in photoreceptor cells expressing both $Rh1^{P37H}$-*GFP* and $perk^{RNAi}$, but not in cells expressing $Rh1^{P37H}$-*GFP* alone (Fig. 6, A and C). Since autophagy is induced by the mutation of *perk* through IRE1 in $Rh1^{P37H}$ expressing photoreceptors, it is possible that wild-type Rh1, but not mutant $Rh1^{P37H}$, is degraded by autophagy. Supporting this, endogenous Rh1 was detected in cytosolic puncta that colocalized with Ref(2)P/P62 and Atg8a in $Rh1^{P37H}$-*GFP* $perk^{RNAi}$ flies. By contrast, $Rh1^{P37H}$-GFP was not detected in Ref(2)P/P62- and Atg8a-positive puncta (Fig. 6, A–D). In TEM images we also observed the presence of autophagosome structures in $Rh1^{P37H}$-*GFP* $perk^{l2}$ photoreceptor cells, but not in $Rh1^{P37H}$-*GFP* photoreceptor cells (Fig. S4 A). Knocking down *ref(2)P/p62* and autophagy-associated genes including *atg1*, *atg9*, and *atg18* largely increase wild-type Rh1 levels in $Rh1^{P37H}$-*GFP* $perk^{RNAi}$ flies. As was seen when we blocked the IRE1/XBP1 signaling pathway, disrupting autophagy did not affect $Rh1^{P37H}$-GFP levels (Fig. 6, E–H). Moreover, knocking down *ref(2)P/p62* reduced the number of Atg8a-positive puncta without affecting the aggregation of wild-type Rh1. This suggests that this selective autophagy occurs downstream of rhodopsin misfolding and/or ubiquitination (Fig. 6 C).

Since autophagy is a general degradation system involved in the turnover of proteins in multiple cellular components, we asked if the autophagy observed in $Rh1^{P37H}$-*GFP* $perk^{l2}$ photoreceptor cells is selective for components of the ER. We drove expression of GFP reporters specific for different subcellular compartment (ER, mitochondria, and cytosol) via the *ninaE* promoter in $Rh1^{P37H}$-*GFP* $perk^{RNAi}$ flies. Levels of ER-GFP were dramatically reduced in $Rh1^{P37H}$-*GFP* $perk^{RNAi}$ flies, whereas reporters specific for mitochondria (mito-GFP) or cytosolic GFP were only slightly reduced. This may reflect the unhealthy state of photoreceptor cells under chronic ER stress (Fig. S4, B–H). In addition to Ref(2)P/P62, two homologs of ER-phagy receptors functioning in mammalian cells, *trp1/sec62* (Fumagalli et al., 2016) and *atl/atl3* (Chen et al., 2019), were also induced in $Rh1^{P37H}$-*GFP* $perk^{RNAi}$ flies. This also could be reversed by knocking down *ire1* (Fig. S4 I). In contrast, the expression of two fly homologs of mammalian mitophagy receptors, *nipsnap* (Princely Abudu et al., 2019) and *phb2* (Wei et al., 2017), were not affected (Fig. S4 I). These data suggest that selective autophagy of ER is induced when the PERK pathway is blocked, and that this autophagy is responsible for reducing wild-type Rh1 in $Rh1^{P37H}$-*GFP* $perk^{RNAi}$ flies.

$Rh1^{P37H}$-GFP is degraded by the UPS system, which is impaired in *perk* mutant cells

Misfolded membrane proteins are recognized by ER chaperons and removed from the ER via a ubiquitin-proteasome system (UPS)-mediated degradation process called ER-associated degradation (ERAD; Meusser et al., 2005; Vembar and Brodsky, 2008). Therefore, the accumulation of mutant $Rh1^{P37H}$ protein may result from an impairment of the ubiquitin/proteasome degradation system. We first tested if the ubiquitination machinery was disrupted in $Rh1^{P37H}$-*GFP* $perk^{RNAi}$ photoreceptor cells. However, both total cellular ubiquitinated proteins and ubiquitinated $Rh1^{P37H}$-GFP accumulated in $Rh1^{P37H}$-*GFP* $perk^{RNAi}$ flies compared with $Rh1^{P37H}$-*GFP* controls (Fig. 7, A and B). These data indicate that proteasome activity in $Rh1^{P37H}$-*GFP* $perk^{RNAi}$ photoreceptor cells may be reduced. To test this hypothesis, we used a proteasome activity reporter, GFP-Flag-Cl1,

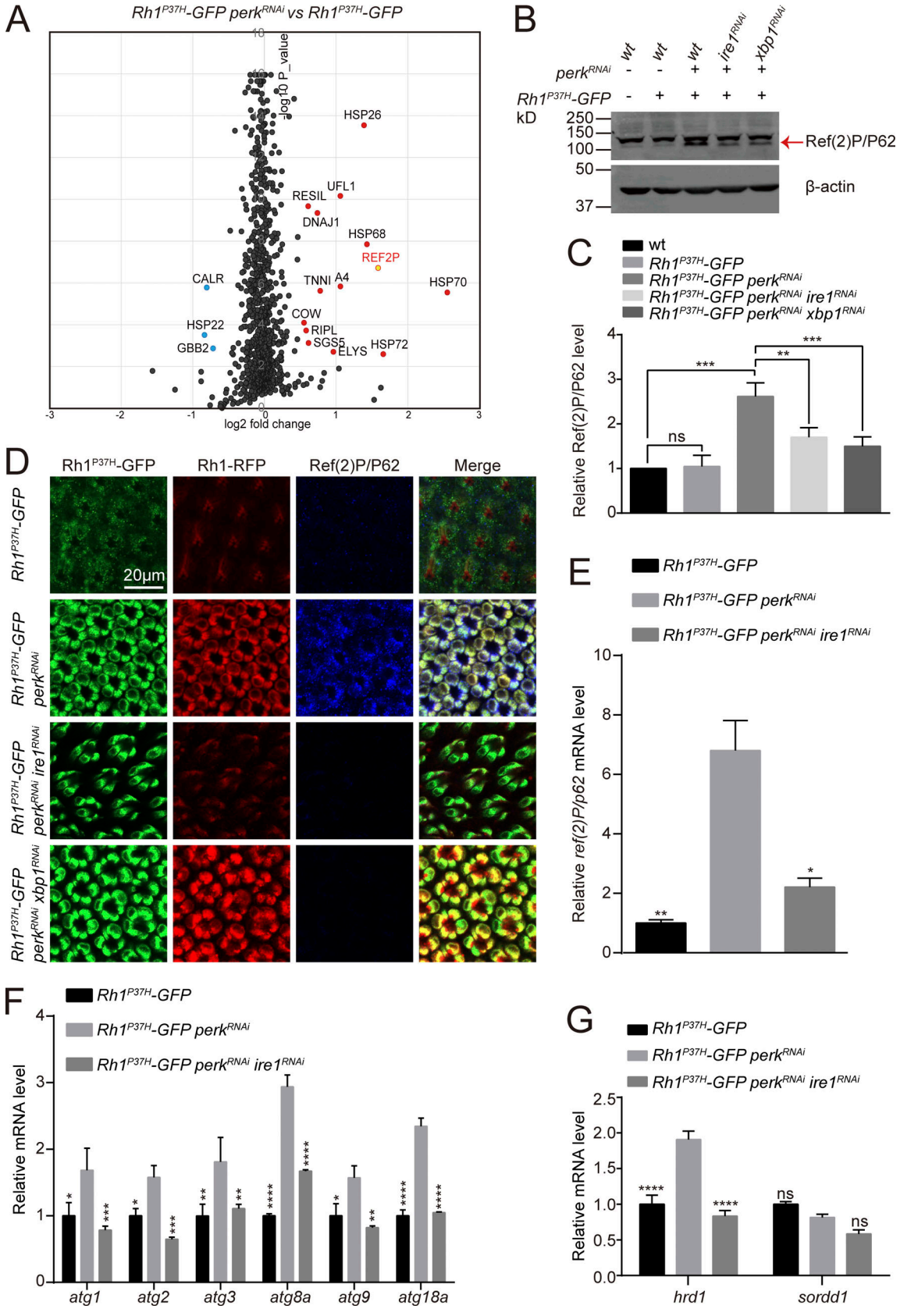

Figure 5. **Autophagy is induced by blocking PERK in *Rh1^{P37H}* photoreceptor cells. (A)** Proteomic profiling comparing protein levels in retinas of *Rh1^{P37H}-GFP perk^{RNAi}* (*GMR-Gal4/UAS-perk^{RNAi} Rh1^{P37H}-GFP*) and *Rh1^{P37H}-GFP* flies (Tandem Mass Tag-LC MS/MS assay). A total of 1,339 proteins were confidently identified (at least two unique peptides per protein). A subset of proteins up- or downregulated in *Rh1^{P37H}-GFP perk^{RNAi}* cells are highlighted by protein

identification. **(B and C)** Western blotting confirmed that Ref(2)P/P62 was upregulated in *Rh1^{P37H}-GFP perk^{RNAi}* flies. This was abolished by expression of *ire1^{RNAi}* and *xbp1^{RNAi}*. Ref(2)P/P62 protein is indicated by the red arrow. Error bars indicate SEM (n = 6); ns, not significant, **P < 0.01, ***P < 0.001 (one-way ANOVA, Sidak's multiple comparisons test). **(D)** Tangential views of retina expressing Rh1^{P37H}-GFP (green) and Rh1-RFP (red) with *perk^{RNAi}* and/or *ire1^{RNAi}/xbp1^{RNAi}* staining against Ref(2)P/P62 (blue). Scale bar, 20 µm. **(E)** qPCR analysis of *ref(2)P/p62* mRNA levels in *Rh1^{P37H}-GFP perk^{RNAi}* and *Rh1^{P37H}-GFP perk^{RNAi} ire1^{RNAi}* retinas compared with *Rh1^{P37H}-GFP* controls. Error bars indicate SEM (n = 3); *P < 0.1, **P < 0.01 (one-way ANOVA, Sidak's multiple comparisons test). **(F)** qPCR analysis showed that mRNA levels of autophagy-related genes (including *atg1*, *atg2*, *atg3*, *atg8a*, *atg9*, and *atg18a*) were upregulated in the retina of *Rh1^{P37H}-GFP perk^{RNAi}* flies, compared with *Rh1^{P37H}-GFP* and *Rh1^{P37H}-GFP perk^{RNAi} ire1^{RNAi}* retina. Error bars indicate SEM (n = 3); *P < 0.1, **P < 0.01, ***P < 0.001, ****P < 0.0001 (two -way ANOVA, Sidak's multiple comparisons test). 1-d-old flies of indicated genotypes were used. **(G)** qPCR analysis showed that mRNA levels of the ER-associated E3 ligase, *hrd1* (bot not *sordd1*) was upregulated in the retina of *Rh1^{P37H}-GFP perk^{RNAi}* flies, compared with *Rh1^{P37H}-GFP* and *Rh1^{P37H}-GFP perk^{RNAi} ire1^{RNAi}* retina. Error bars indicate SEM (n = 3); ns, not significant, ****P < 0.0001 (two-way ANOVA, Sidak's multiple comparisons test). 1-d-old flies of indicated genotypes were used. Source data are available for this figure: SourceData F5.

which contains a short degron fragment (CL1) that is degraded by the ubiquitin-proteasome system (Gilon et al., 1998; Nonaka and Hasegawa, 2009). GFP-Flag-Cl1 was linked to mCherry (as an internal control) via a self-cleaving peptide T2A. The reporter was then expressed in photoreceptor cells via the *ninaE* promoter. Compared with wild-type flies, GFP-Flag-CL1 levels were slightly increased in *Rh1^{P37H}-GFP* flies. Levels of GFP-Flag-CL1 were dramatically elevated when the proteasomal subunit *prosβ1* was knocked down (Fig. 7, C and D). Importantly, as seen with blocking the proteasomal subunit, *perk* mutation largely stabilized GFP-FLAG-CL1 in *Rh1^{P37H}-GFP* flies (Fig. 7, C and D). These data suggest that the UPS system is impaired when PERK is blocked during ER stress. Moreover, expression of the E3 ligase SORDD1 (Xu et al., 2020) in *Rh1^{P37H}-GFP perk^{RNAi}* photoreceptor cells prevented the accumulated Rh1^{P37H}-GFP (Fig. 7, E and F) but did not affect wild-type Rh1 levels. This is consistent with SORDD1 only being involved in the degradation of misfolded rhodopsin (Xu et al., 2020).

The Ref(2)P/P62 protein is an adaptor that binds ubiquitinated proteins and autophagy components, thereby serving as a linker between the autophagy machinery and its targets. Considering the fact that total ubiquitination levels increased in *Rh1^{P37H}-GFP perk^{RNAi}* flies, we reasoned that the accumulation of ubiquitinated ER proteins initiated the ER-phagic degradation of wild-type Rh1. Consistent with induction of the ERAD ubiquitin ligase, Hrd1, ubiquitinated membrane proteins accumulated in *Rh1^{P37H}-GFP perk^{RNAi}* flies. This could be reversed by knocking down *ire1* (Fig. S4 J). To further test this hypothesis, we overexpressed the general cytosolic deubiquitinase, USP15-31, in *Rh1^{P37H}-GFP perk^{RNAi}* flies and found that USP15-31 restored levels of wild-type Rh1 in *Rh1^{P37H}-GFP perk^{RNAi}* flies without affecting the levels of Rh1^{P37H}-GFP (Fig. 7, G and H). Further, total cellular ubiquitination levels were largely decreased in *Rh1^{P37H}-GFP perk^{RNAi}* flies when USP15-31 was overexpressed, whereas ubiquitination levels of Rh1^{P37H}-GFP were unaffected (Fig. 7, I and J). These data provided further evidence that Rh1 degradation is regulated by Ref(2)P/P62-mediated selective autophagy, which is different from UPS-mediated degradation of Rh1^{P37H}-GFP.

PERK prevents retinal degeneration in the *ninaE^{G69D}* model of adRP

Since inhibiting PERK induced ER-phagic degradation of wild-type Rh1, and increased the cytotoxicity of misfolded Rh1^{P37H}, it is possible that induction of PERK could suppress autophagy and alleviate retinal degeneration associated with mutations in rhodopsin. To test this hypothesis, we used a classic adRP model in which the *ninaE^{G69D}* mutation leads to age-dependent degeneration of photoreceptor cells (Colley et al., 1995; Kurada and O'Tousa, 1995). We first examined if autophagy is induced by the *ninaE^{G69D}* mutation. Consistent with previous results using *Rh1^{P37H}*, the *sxbp1/uxbp1* ratio was increased in *ninaE^{G69D}* flies, indicating activation of the UPR (Fig. 8 and Fig. 9 A). *ninaE^{G69D}* photoreceptor cells also exhibited large increases in *ref(2)P/p62* mRNA levels, as well as Ref(2)P/P62- and Atg8-positive puncta, compared with wild-type controls (Fig. 9, B–D and Fig. S5 J). Moreover, ER-GFP but not mito-GFP or cytosolic GFP colocalized with Ref(2)P/P62 in *ninaE^{G69D}* flies (Fig. S5, A–D), and levels of ER-GFP but not mito-GFP protein were significantly reduced in *ninaE^{G69D}* flies (Fig. S5, E–H). To test the role of Ref(2)P/P62 in inducing autophagy in *ninaE^{G69D}* photoreceptor cells, we used the CRISPR-CAS9 system to generate a *ref(2)P/p62* mutant fly (Fig. S5 I). The *ref(2)P^{m}* mutation itself did not affect autophagy in photoreceptor cells. However, loss of Ref(2)P/P62 in *ninaE^{G69D}* photoreceptor cells largely abolished the formation of Atg8a puncta (Fig. S5 J). These data indicate that the selective autophagy of ER is induced in the *ninaE^{G69D}* model of adRP and is involved in general degradation of the ER compartment. Importantly, overexpressing PERK in photoreceptor cells under control of the endogenous *trp* (*transient receptor potential*) promoter greatly reduced levels of Ref(2)P/P62 in aged *ninaE^{G69D}* photoreceptor cells, compared to wild-type controls (Fig. 9, C and D). *ninaE^{G69D}* flies exhibited phenotypes consisted with severe retinal degeneration including reduced ERG responses, and loss of rhabdomeres and photoreceptor cells ∼30 d after eclosion (Fig. 9, E–H). Expression of PERK in photoreceptor cells completely restored ERG responses and prevented the loss of photoreceptor cells in 30-d-old *ninaE^{G69D}* flies (Fig. 9, E–H). In contrast, overexpression of ATF4 did not affect the loss of ERG and photoreceptor cells in the *ninaE^{G69D}* mutants (Fig. 9, E–H). Consistent with our previous results, these data demonstrate that PERK suppresses adRP independent of ATF4.

Discussion

In conclusion, we found that PERK is important for maintaining rhodopsin homeostasis during prolonged ER stress. In photoreceptor cells expressing misfolded Rh1^{P37H}, the continuous activation of PERK attenuates IRE1/XBP1 signaling, which is adapted to this chronic ER stress, in an eIF2α-dependent manner.

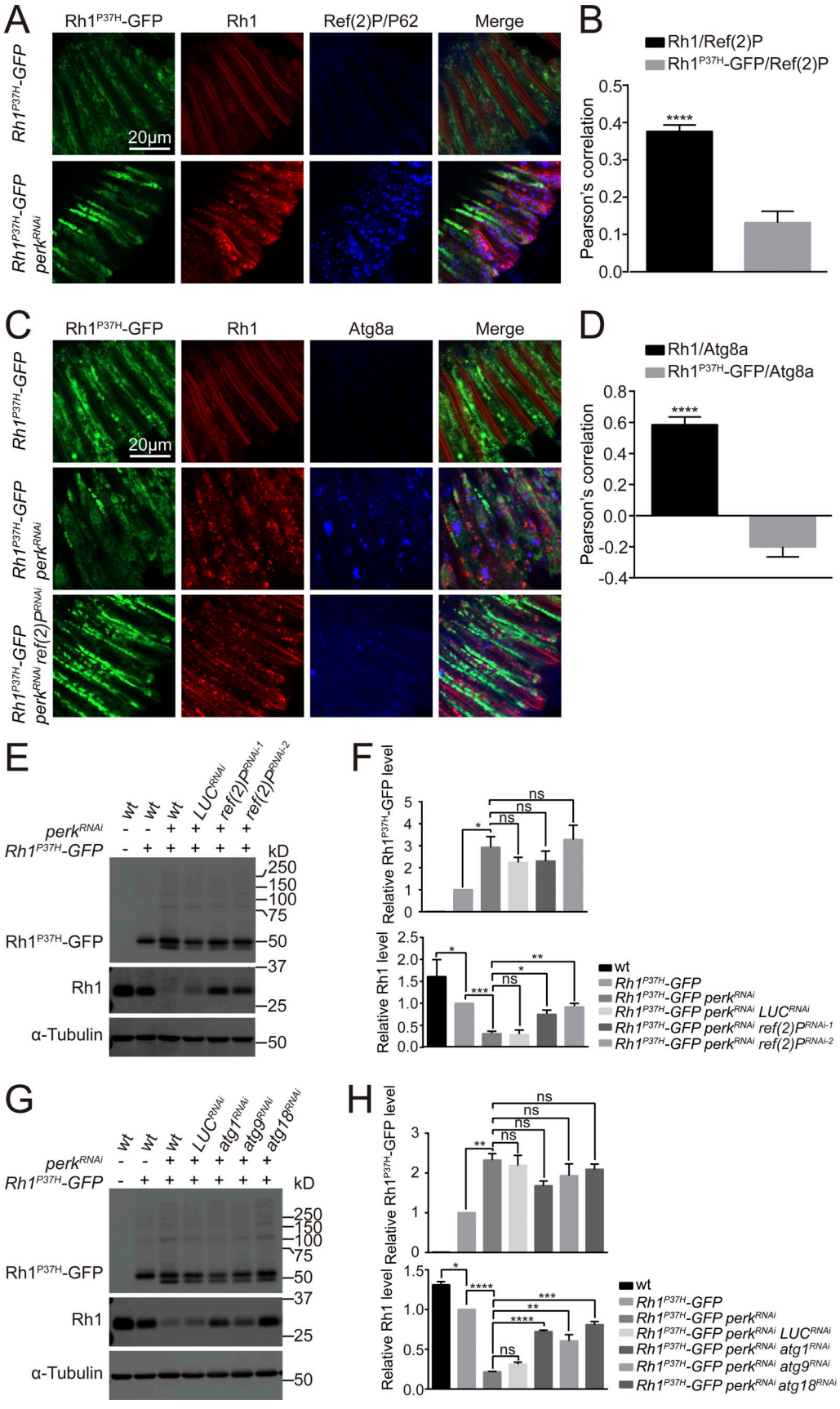

Figure 6. **Wild-type Rh1 but not Rh1^{P37H} is degraded through autophagy. (A–D)** Wild-type Rh1, but not Rh1^{P37H} colocalized with Ref(2)P/P62 and Atg8a in *Rh1^{P37H}-GFP perk^{RNAi}* flies. **(A)** Longitudinal views of photoreceptor cells labeled for GFP (Rh1^{P37H}-GFP, green), RFP (Rh1-RFP, red), and Ref(2)P/P62 (blue). Scale

bar, 20 µm. **(B)** Quantification of the co-localization between Rh1^{P37H}-GFP or Rh1-RFP and Ref(2)P/P62 in *Rh1^{P37H}-GFP perk^{RNAi}* photoreceptor cells. Error bars indicate SEM (n = 3); ****P < 0.0001 (Student's unpaired t test). **(C)** Immune staining of photoreceptor cells against GFP (Rh1^{P37H}-GFP, green), RFP (Rh1-RFP, red), and Atg8a (blue). Scale bar, 20 µm. **(D)** Quantification of the co-localization between Rh1^{P37H}-GFP or Rh1-RFP and Atg8a in *Rh1^{P37H}-GFP perk^{RNAi}* photoreceptor cells. Error bars indicate SEM (n = 3); ****P < 0.0001 (Student's unpaired t test). **(E and F)** Western blotting showed that knocking down *ref(2)P/p62* significantly blocked the reduction of wild-type Rh1 without affecting the accumulation of Rh1^{P37H}-GFP in *Rh1^{P37H}-GFP perk^{RNAi}* retina. Two independent *ref(2)P/p62^{RNAi}* lines were used, and *LUC^{RNAi}* was used as a control. Error bars indicate SEM (n = 3); ns, not significant, *P < 0.1, **P < 0.01, ***P < 0.001 (one-way ANOVA, Sidak's multiple comparisons test). **(G and H)** Western blot analysis against Rh1^{P37H}-GFP and endogenous Rh1 showed that *atg1^{RNAi}*, *atg9^{RNAi}*, and *atg18^{RNAi}* suppressed *perk^{RNAi}*-mediated decreases in wild-type Rh1 in *Rh1^{P37H}-GFP* photoreceptor cells. Error bars indicate SEM (n = 3); ns, not significant, *P < 0.1, **P < 0.01, ***P < 0.001, ****P < 0.0001 (one-way ANOVA, Sidak's multiple comparisons test). *LUC^{RNAi}* was used as a control line, and α-tubulin was used as a loading control. 1-d-old flies of indicated genotypes were used. Source data are available for this figure: SourceData F6.

However, when PERK is blocked, global translation is no longer inhibited by phosphorylated eIF2α. This increases the burden on the proteasome and reduces degradation of Rh1^{P37H} by ERAD. By contrast, in the absence of the PERK pathway, IRE1/XBP1 signaling remains activated, inducing multiple autophagy-related genes including *ref(2)P/p62*. Together with the accumulation of ubiquitinated proteins due to proteasome overload, the upregulation of these autophagy-related genes induces the selective autophagy of ER. This promotes the degradation of wild-type rhodopsin that has accumulated in the ER, ultimately triggering photoreceptor cell death (Fig. 8).

The three branches of the UPR (IRE1, PERK, and ATF6) are simultaneously induced in response to cellular stress. However, in the context of chronic ER stress, the three UPR pathways are differentially affected. This is particularly true for the IRE1 and PERK branches, which may be due to interactions between these two signaling pathways. During development of plasma cells, IRE1 is robustly activated, whereas activation of PERK is suppressed by Ufbp1 (Ufm1-binding protein; Zhu et al., 2019). Under prolonged ER stress, the activities of IRE1 and ATF6 are attenuated, whereas PERK signaling persists (Lin et al., 2007). In cultured cells, translational attenuation by PERK facilitates IRE1 during the early adaptive phase of the UPR (Moore and Hollien, 2015), but during the prolonged UPR stage, IRE1 activity is attenuated by PERK/eIF2α-dependent and ATF4-independent translational inhibition to turn off IRE1 activity (Chang et al., 2018). In chronic ER stress induced by Rh1^{P37H}, blocking PERK signaling activates *xbp1* splicing and thus the transcription function of XBP1. Consistent with results seen with pharmacologically induced ER stress, this IRE1/XBP1 re-activation is mediated by loss of translational inhibition in *perk* mutants, as slowing translation by expressing short-hairpin RNAs against *eIF3b* and *eIF4G* suppressed XBP1 over-activation by loss of *perk*. This suggests the mechanisms of prolonged ER-stress adaptation through attenuation of IRE1 by PERK are conserved across species. However, in contrast to cultured cells, where pharmacological ER stress attenuates IRE1 through PERK to trigger apoptosis, in photoreceptor cells in vivo ER-stress adaptation through attenuation of IRE1 is cytoprotective. In Rh1^{P37H}-expressing photoreceptor cells, severe cell death was induced by mutations of both *perk* and *eIF2Bα*, whereas the cells survived upon Rh1^{P37H} expression alone. Further, IRE1-mediated *xbp1* splicing was boosted, and wild-type rhodopsin was largely degraded by blocking of PERK in Rh1^{P37H}-expressing cells. Knocking down *ire1* or *xbp1* completely rescued this rhodopsin loss. Therefore, our present study suggests that the downregulation of IRE1 by PERK is cytoprotective during chronic ER stress.

In both yeast and neuroblastoma cells, induction of ER stress activates autophagy in an IRE1-dependent manner (Ogata et al., 2006; Yorimitsu et al., 2006). In *Drosophila* neurons, ectopic overexpression of IRE1 was sufficient to induce autophagy and triggered neuron death (Yan et al., 2019). As a cellular quality control mechanism for clearance of proteins and organelles, loss or over-activated of autophagy can trigger neuronal cell death under certain pathological conditions (Hara et al., 2006; Komatsu et al., 2006; Wang et al., 2009). Besides clearing misfolded proteins, autophagy can degrade normal folded proteins or undamaged organelles derived from imbalanced proteostasis; this ultimately disrupts cellular function (Berry and Baehrecke, 2007; Doherty and Baehrecke, 2018). A previous study found that autophagy flux is elevated in *Rho^{P23H}*/+ mice, and inhibiting autophagy reduces retinal degeneration caused by protein misfolding (Yao et al., 2018). However, how autophagy is induced in this adRP model remains unclear, and the molecular mechanisms linking autophagy and *Rho^{P23H}*-induce photoreceptor cell degeneration remains a mystery. In our study, we first observed in the retinas of *Rh1^{P37H}-GFP perk^{RNAi}*: (1) dramatic accumulations of the autophagic substrate Ref (2)P/P62 and the autophagy marker LC3/ATG8, (2) transcriptional activation of multiple autophagy-related genes, and (3) a large increase in autophagy flux. Further evidence showed that downregulation of IRE1/XBP1 signaling reversed the induction of autophagy in *Rh1^{P37H}-GFP perk^{RNAi}* photoreceptor cells. Finally, in the fly adRP model *ninaE^{G69D}*, accumulation of Ref(2)P/P62- and Atg8-positive puncta was associated with *xbp1* splicing. Studies in both *Drosophila* and mammalian cells have demonstrated that induction of PERK/eIF2α induces autophagy (B'Chir et al., 2013; Nagy et al., 2013), indicating that PERK/eIF2α signaling could regulate autophagy through different signaling pathways. We conclude that the uncontrolled activation of IRE1/XBP1 signaling could induce autophagy under prolonged ER stress.

Degradation of misfolded ER proteins via ERAD, which involves the ubiquitin–proteasome system, is a major mechanism for maintaining proper proteostasis of the ER (Walter and Ron, 2011). Maintaining proteostasis of ER proteins may also require the second degradative system of the cell, the autophagy-lysosome pathway through selective ER autophagy, ER-phagy (Khaminets et al., 2015). Since ER-phagy was originally described, it has been shown that several ER-phagy receptors interact with the autophagy-related protein LC3/ATG8 to recruit the autophagosome and promote the selective clearance of

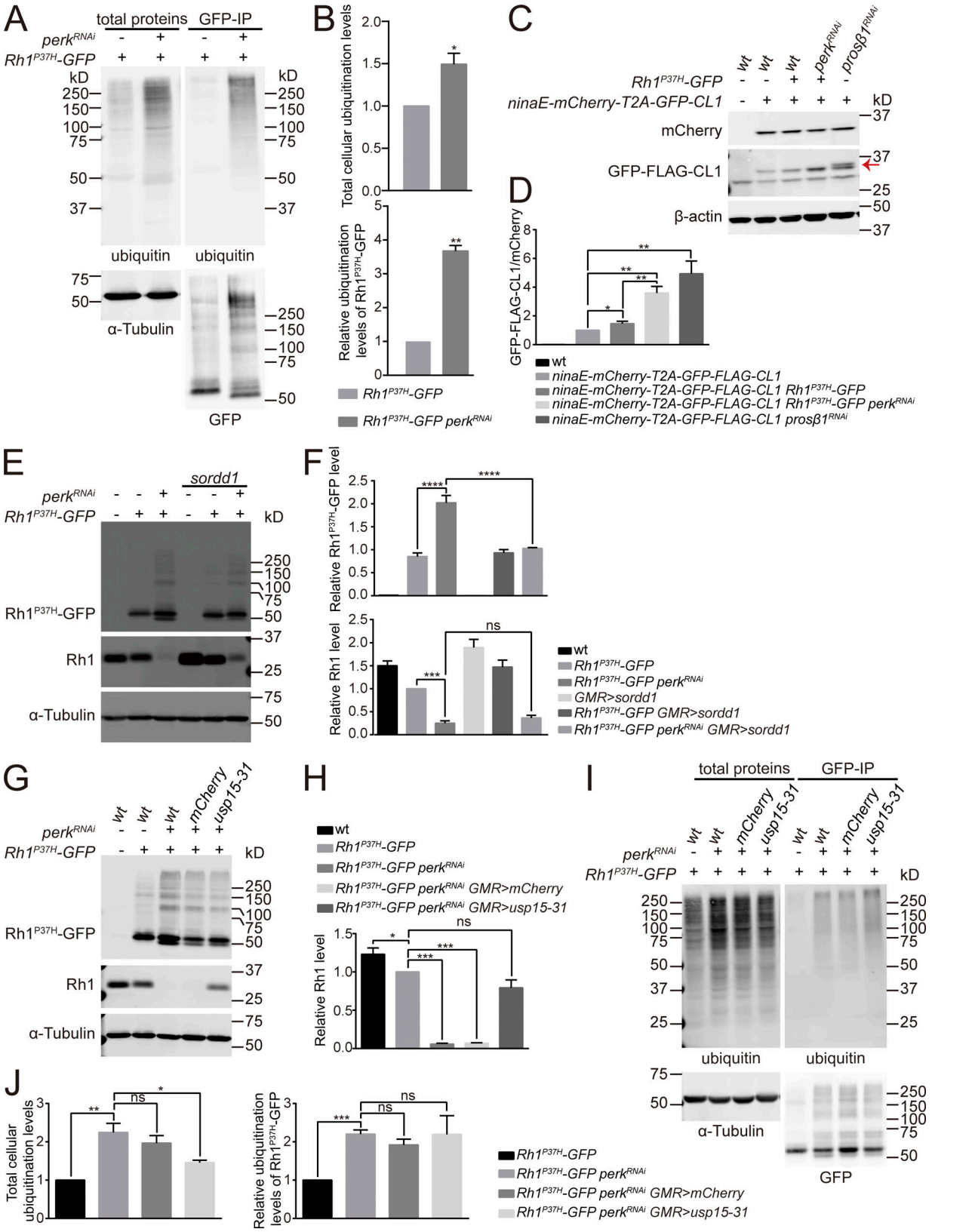

Figure 7. **The ubiquitin-proteasome system (UPS) is impaired upon blocking PERK in adRP photoreceptors. (A)** Accumulation of ubiquitinated proteins in *Rh1*^{P37H}*-GFP perk*^{RNAi} flies. Head lysate of *Rh1*^{P37H}*-GFP* and *Rh1*^{P37H}*-GFP perk*^{RNAi} flies were immunoprecipitated with anti-GFP beads and stained against ubiquitin and GFP. **(B)** Quantification of total cellular ubiquitination levels (upper panel), and relative ubiquitination levels of Rh1^{P37H}-GFP (lower panel) in A. Error bars indicate SEM (n = 3); *P < 0.1, **P < 0.01 (Student's unpaired t test). **(C)** Western blotting against GFP and mCherry to examine proteasome activity in *Rh1*^{P37H}*-GFP perk*^{RNAi} flies. The *ninaE* promoter was used to drive *mCherry-T2A-GFP-FLAG-Cl1* expression. Knock down of the proteasome subunit by *prosβ1*^{RNAi}

was used as a positive control. GFP-FLAG-CL1 protein is indicated by the red arrow. **(D)** Quantification of GFP-FLAG-CL1 and mCherry ratio in C. Error bars indicate SEM (n = 3); *P < 0.1, **P < 0.01 (one-way ANOVA, Sidak's multiple comparisons test). **(E and F)** Western blot analysis showed that overexpression of SORDD1 in photoreceptor cells reduced Rh1^{P37H}-GFP specifically upon loss of *perk* without affecting the Rh1 levels. Error bars indicate SEM (n = 3); ns, not significant, ***P < 0.001, ****P < 0.0001 (one-way ANOVA, Sidak's multiple comparisons test). **(G and H)** Western blot analysis showed that USP15-31 restored Rh1 levels in *Rh1^{P37H}-GFP perk^{RNAi}* flies without affecting the levels of Rh1^{P37H}-GFP. Error bars indicate SEM (n = 3); ns, not significant, *P < 0.1, ***P < 0.001 (one-way ANOVA, Sidak's multiple comparisons test). **(I)** Overexpression of USP15-31 reduced the accumulation of ubiquitinated proteins in *Rh1^{P37H}-GFP perk^{RNAi}* flies, without affecting the ubiquitination levels of Rh1^{P37H}-GFP. Head lysates of *Rh1^{P37H}-GFP*, *Rh1^{P37H}-GFP perk^{RNAi}*, *Rh1^{P37H}-GFP perk^{RNAi} mCherry* (*GMR-Gal4/UAS-mCherry;UAS-perk^{RNAi}/Rh1^{P37H}-GFP*) and *Rh1^{P37H}-GFP perk^{RNAi} usp15-31* (*GMR-Gal4/UAS-usp15-31;UAS-perk^{RNAi}/Rh1^{P37H}-GFP*) flies were immunoprecipitated with anti-GFP beads and stained against ubiquitin and GFP. **(J)** Quantification of total cellular ubiquitinated proteins (left panel), and relative ubiquitination levels of Rh1^{P37H}-GFP (right panel) in I. Error bars indicate SEM (n = 3); ns, not significant, *P < 0.1, **P < 0.01, ***P < 0.001 (one-way ANOVA, Sidak's multiple comparisons test). 1-d-old flies of indicated genotypes were used. Source data are available for this figure: SourceData F7.

excessive membrane portions of the ER (An et al., 2019; Fumagalli et al., 2016; Grumati et al., 2017; Khaminets et al., 2015). However, discovery of these ER-phagy receptors did not reveal whether ER-phagy is directly involved in the clearance of misfolded proteins (in parallel or complementary to ERAD), thereby playing a role in the UPR. In our present study, we present evidence that ER-phagy is induced by prolonged ER stress through imbalanced UPR activation, and that ER-phagy is involved in the selective clearance of ER proteins. As a scaffold protein, the autophagic adapter Ref(2)P/P62 delivers ubiquitinated proteins for selective autophagic degradation by: (1) interacting with LC3/ATG8 through its LIR region, and (2) interacting with ubiquitinated proteins through its ubiquitin-associated (UBA) domain (Moscat and Diaz-Meco, 2012; Nezis et al., 2008). In prolonged ER stress (both *Rh1^{P37H}-GFP perk^{RNAi}* and *ninaE^{G69D}* photoreceptor neurons), membrane proteins including rhodopsin get stuck and ubiquitinated in ER. Thus Ref(2)P/P62 and LC3/ATG8 proteins also accumulate, and wild-type rhodopsin and ER-GFP can be detected within Ref(2)P/P62 puncta. By contrast, the mitochondrial reporter mito-GFP did not associate with these puncta. In both *Rh1^{P37H}-GFP perk^{RNAi}* and *ninaE^{G69D}* photoreceptor cells, levels of ER-GFP and wild-type rhodopsin were dramatic reduced, whereas proteins in other cellular compartments (mito-GFP and cytosolic GFP) were less affected. When we knocked down *ref(2)P/p62* or autophagy-relative genes, this UPR induced autophagy was disrupted and degradation of wild-type rhodopsin was prevented. Our results suggested that tuning down selective autophagy may protect against retinal degeneration. Interestingly, it has recently been reported that disrupting the interaction between Ref(2)P/P62 and Atg8a increases the tolerance to oxidative stress and reduces levels of aging-associated mitochondrial superoxide in *Drosophila* (Bhattacharjee et al., 2022).

Despite being caused by different insults, misfolded membrane proteins accumulated in the ER and were removed through ERAD via ubiquitination. The accumulation of misfolded proteins could exert a dominant negative effect on wild-type ER proteins, as illustrated by the dominant mutations in

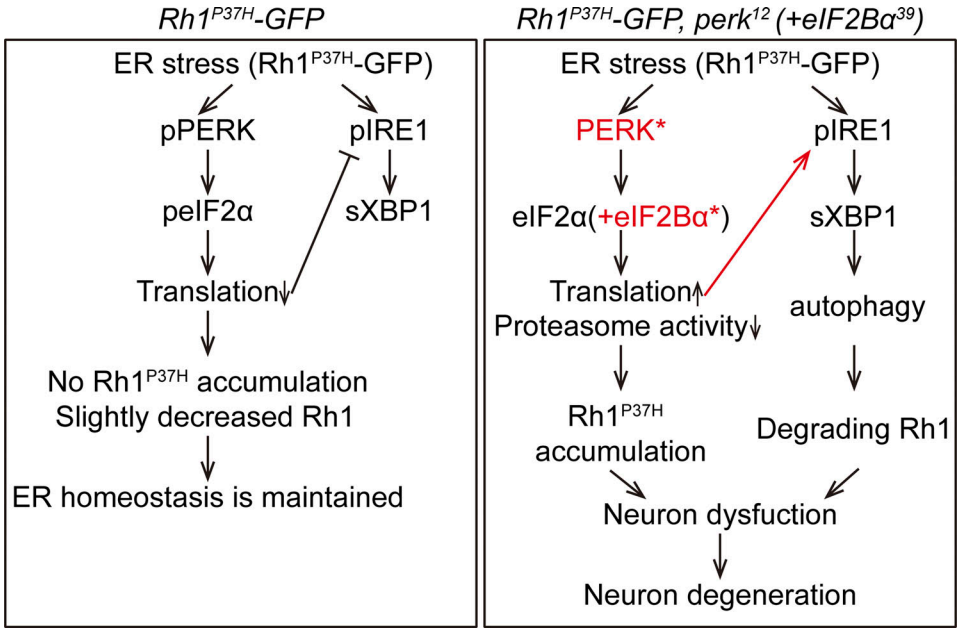

Figure 8. **Working model of cell protective role of PERK in prolonged ER stress triggered by misfolded Rh1^{P37H}.** On the left we illustrate that PERK signaling plays a central role in maintaining rhodopsin homeostasis and cellular function in cells expressing Rh1^{P37H}. On the right we show that deficiency in the PERK pathway (*perk^{12}* or *eIF2Bα^{39}* mutation) de-inhibits translation and over-activates IRE1, leading to the accumulation of Rh1^{P37H} due to insufficient proteasome activity and degradation of wild-type Rh1 through induction of autophagy. This ultimately causes neuron dysfunction and degeneration.

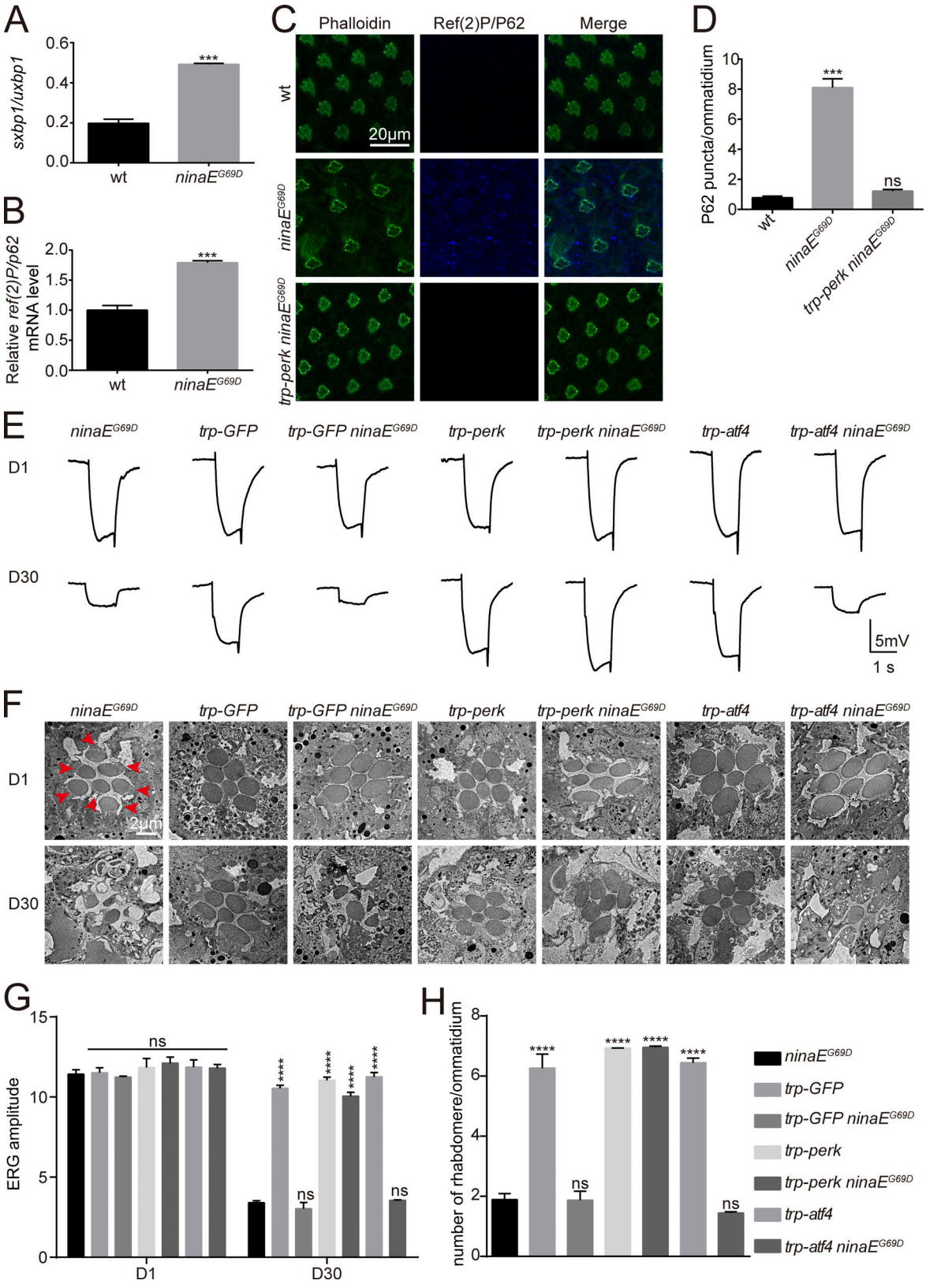

Figure 9. **PERK prevents retinal degeneration in the *ninaE*^{G69D} model of adRP. (A and B)** qPCR analysis of the *sxbp1/uxbp1* ratio (A) and mRNA levels of *ref(2)P/p62* (B) demonstrated that the IRE1/XBP1/autophagy axis was activated in *ninaE*^{G69D} photoreceptor cells. Error bars indicate SEM (n = 3); ***P < 0.001 (Student's unpaired t test). **(C and D)** Immunostaining of photoreceptor cells against Ref(2)P/P62 showed an increase of Ref(2)P/P62 puncta in *ninaE*^{G69D} photoreceptor cells. This was abolished by ectopic expression of PERK. Phalloidin served as an ommatidia maker. Error bars indicate SEM (n = 3); ns, not significant, ***P < 0.001 (one-way ANOVA, Sidak's multiple comparisons test). **(E)** Representative ERG recordings of 1-d-old and 30-d-old flies showed that

PERK but not ATF4 prevented the loss of visual response in *ninaE*^{G69D} flies. Flies with indicated genotypes were exposed to a 1-s pulse of orange light after 2 min of dark adaptation. **(F)** Representative TEM images of 1-d-old and 30-d-old eye tangential sections. Genotypes are indicated. Rhabdomeres are indicated by red arrows. Scale bar, 2 µm. **(G)** Statistical analysis of the amplitude of ERG recordings for 1-d-old and 30-d-old flies from E. Error bars indicate SEM (n = 6); ns, not significant, ****P < 0.0001 (two-way ANOVA, Sidak's multiple comparisons test). **(H)** Quantification of the number of rhabdomeres per ommatidia in F. Sections from three 30-d-old flies of each genotype were used for quantification. ns, not significant, ****P < 0.0001 (one-way ANOVA, Sidak's multiple comparisons test). All flies were in white eye background, and were raised in 12-h light/12-h dark (L/D) cycles at 25°C.

opsin genes (Colley et al., 1995; Mendes and Cheetham, 2008; Rajan and Kopito, 2005; Saliba et al., 2002). By conducting a genome-wide loss of function screen, PERK and eIF2Bα were found to play a key role in maintaining levels of wild-type rhodopsin in heterozygous *Rh1*^{P37H} mutants. Further, disruption of the selective autophagy through inactivation of Ref(2)P/P62 prevented the dominant effects of Rh1^{P37H} , and maintained normal levels of wild-type Rh1. Although it has been reported that misfolded CFTR (Cystic Fibrosis Transmembrane Conductance Regulator), and gonadotropin-releasing hormone receptor (GnRHR), are resistant to ERAD and cleared by an ER-associated autophagy (He et al., 2021; Houck et al., 2014), ER-associated autophagy had little effect on the clearance of mutant rhodopsin. Elevated ER-phagy was associated with the accumulation of Rh1^{P37H}, and interruption of autophagy had no effect on Rh1^{P37H} accumulation. This is consistent with results seen in mice that inhibiting autophagy reduced the cytotoxicity of misfolded Rho^{P23H} (Yao et al., 2018). Studies in both *Drosophila* and mice have demonstrated that increasing ERAD by either induction of E3 ligases or proteasome activity reduced mutated rhodopsin and is cytoprotective (Kang and Ryoo, 2009; Lobanova et al., 2018; Xu et al., 2020). Indeed, blocking PERK signaling resulted in the accumulation of ubiquitinated proteins, preventing the proteasome from degrading its normal target such as GFP-Flag-Cl1. This increased burden on the proteasomal degradation machinery has been implicated in the pathology of multiple inherited retinal degeneration diseases (Lobanova et al., 2013). Specific ubiquitination of Rh1^{P37H} by the E3 ligase SORDD1 dramatically decreased the accumulation of misfolded Rh1^{P37H} in *Rh1*^{P37H}*-GFP perk*^{RNAi} photoreceptor cells, but still reduced wild-type Rh1. On the contrary, blocking ER-phagy restored wild-type Rh1 but did not affect Rh1^{P37H}, supporting the notion that Rh1^{P37H} and wild-type Rh1 are cleared by different degradation machineries. Moreover, expressing the deubiquitinase USP15-31, which largely alleviated levels of cytosolic ubiquitination but did not affect ubiquitination of Rh1^{P37H}, prevented the ER-phagic degradation of wild-type Rh1 but not the accumulation of Rh1^{P37H}. The accumulation of ubiquitinated proteins upon proteasome overload in prolonged ER stress, along with upregulation of Ref(2)P/P62, promoted the selective autophagy of general ER proteins including wild-type rhodopsin, whereas unfolded Rh1^{P37H} was not a substrate of this selective autophagy. Rh1^{P37H} may be segregated into a distinct ER substructure. The observation that only wild-type Rh1 but not Rh1^{P37H} was detected in Ref(2)P/P62 puncta further supports this.

Impaired processing of ubiquitinated proteins has been reported in several mouse models of retinal degeneration (Lobanova et al., 2018; Lobanova et al., 2013), as we found in *Rh1*^{P37H}*-GFP perk*^{RNAi} photoreceptor cells. Moreover, photoreceptor degeneration in *Rho*$^{P23H/+}$ mice can be delayed by increasing photoreceptor proteasomal activity through overexpression of the 11S proteasome cap subunit, PA28α or activation of mTORC1 (Lobanova et al., 2018; Wang et al., 2022). Ubiquitin ligases and the upstream ERAD proteins were upregulated through IRE1/XBP1 signaling, which could induce proteasomal overload. This global impairment of proteasomal function precedes photoreceptor cell death (Chiang et al., 2015). As a result of insufficiency of the UPS system, autophagy is elevated to complement proteasome-dependent degradation. The continuously activating IRE1/XBP1 signaling upregulated multiple autophagy-related genes in *Rh1*^{P37H}*-GFP perk*^{RNAi} photoreceptor cells, while in combination with loss of translational inhibition through PERK/eIF2α deficiency, ubiquitinated proteins accumulated. These signals ultimately led to the induction of ubiquitination/P62-mediated selective autophagy. However, the autophagy could not substitute for the UPS system, as Rh1^{P37H} was resistant to autophagy, whereas ER proteins and wild-type Rh1 were found in autophagosomes. This ER-phagy degradation of wild-type Rh1 accelerated the retinal degeneration induced by *Rh1*^{P37H}. In the fly *ninaE*^{G69D} model of adRP, prolonged activation of IRE1/XBP1 signaling was associated with autophagy induction, degradation of normal ER proteins, dysfunction in phototransduction, and retinal degeneration, whereas overexpression of PERK largely suppressed these phenotypes. Supporting this point, *xbp1* deficiency protects against neurodegeneration in transgenic mouse models of Huntington disease (HD) and amyotrophic lateral sclerosis (ALS), likely through the enhancement of autophagy (Hetz et al., 2009; Vidal et al., 2012).

Under ER stress, PERK is activated by oligomerization and autophosphorylation, which enables the phosphorylation of eIF2α, reducing global translational efficiency by blocking 80S ribosome assembly (Harding et al., 1999; Shi et al., 1998). In addition to eIF2α, activated PERK also phosphorylates and activates other targets such as Nrf2 and FOXO, regulating cellular metabolic adaptation and survival in the context of ER stress (Cullinan et al., 2003; Zhang et al., 2013). When ER stress was induced by misfolded rhodopsin Rh1^{P37H}, PERK-eIF2α signaling is key for maintaining rhodopsin homeostasis. Rhodopsin homeostasis was disrupted by mutations in *eIF2Bα*, which regulates eIF2α, as well as in *perk* mutants under mild ER-stress. Expressing the dominant negative form of eIF2α mimicked the phenotype of *perk* mutant in terms of both accumulation of Rh1^{37H} and reduction of wild-type Rh1. Moreover, inhibiting global translation by knocking down *eIF3b* and *eIF4G* abolished the effects of *perk* deficiency on both mutant and wild-type Rh1. Besides reducing global protein biosynthesis, PERK-mediated phosphorylation of eIF2α increases the translation of ATF4 by bypassing upstream open reading frames (uORFs; Harding et al., 2000a). As a transcription factor that activates UPR target genes

associated with protein folding and apoptosis, ATF4 plays an essential role in PERK-mediated UPR (Costa-Mattioli and Walter, 2020). However, ATF4 plays a minor role in maintaining homeostasis of rhodopsin through PERK signaling. First, unlike mutations in *perk* or *eIF2Bα*, animals with complete loss of *atf4* exhibited little changes in both mutant and wild-type rhodopsin. Second, mimicking the increased translation of ATF4 by activation of ATF4 through deletion of uORF did not suppress *perk* mutation-induced accumulation of $Rh1^{37H}$ and reduction of wild-type Rh1. Finally, expression of ATF4 had no effect on the severity of retinal degeneration in the $ninaE^{G69D}$ model, while over-expression of PERK strongly suppressed this retinal degeneration. Besides ATF4, several factors are translationally induced by eIF2α in parallel to ATF4 in both mammalian cells and flies (Andreev et al., 2015; Baird et al., 2014; Brown et al., 2021; Zhou et al., 2008). The fact that translational inhibition by interfering with eIF3b and eIF4G could mimic rhodopsin level phenotypes strongly argues against the possibility that eIF2α-dependent translational induction is required in this PERK signaling.

Protein misfolding and activation of the UPR is emerging as a common mechanism in neurodegeneration diseases. Studies inhibiting the PERK branch of UPR have shown that PERK inhibitors protect against neuronal cell death in models of Alzheimer's disease (AD), Parkinson's disease (PD), and amyotrophic lateral sclerosis (ALS; Celardo et al., 2016; Kim et al., 2013; Moreno et al., 2013). A protective role of PERK in Charcot-Marie-Tooth (CMT) disease has also been demonstrated, as genetic and pharmacological inactivation of Gadd34 (damage-inducible protein 34) antagonizes PERK activity toward eIF2α and improves motor, neurophysiological, and morphologic deficits in mouse models (Scapin et al., 2020). In mouse models of adRP (heterozygous Rho^{P23H}), PERK protects against degeneration of photoreceptor cells (Athanasiou et al., 2017; Chiang et al., 2012a). Consistent with this, loss-of-function *perk* mutations dramatically accelerate retinal degeneration in fly $ninaE^{G69D}$ models (Vasudevan et al., 2020). In contrast, limited ATF4 expression protects photoreceptor cells from Rho^{P23H}-induced retinal degeneration, while conflicting evidence suggests that loss of *ATF4* accelerates retinal degeneration in *Drosophila* $ninaE^{G69D}$ *models* (Bhootada et al., 2016; Vasudevan et al., 2022). Supporting the protective role of PERK but not ATF4 in adRPs, loss of function of PERK led to severe retinal degeneration in $Rh1^{P37H}$-expressing cells, whereas a null ATF4 allele did not. Importantly, overexpression of PERK strongly suppressed retinal degeneration in $ninaE^{G69D}$ flies, whereas ATF4 had no effect. In accordance with the deteriorating role of autophagy, the degenerating $ninaE^{G69D}$ flies exhibit increases in autophagy (in particular ER-phagy) and activation of PERK prevents autophagy, suggesting that reduced autophagy flux is part of the protective mechanism of PERK (Qiu et al., 2019; Yao et al., 2018). Our findings indicate that prolonging PERK activities represent a valid therapeutic target in ER stress-related neuropathies such as adRP.

Materials and methods

Fly stocks

The following fly lines were obtained from the Bloomington Stock Center: *P{UAS-LUC.VALIUM10}attP2* (LUC^{RNAi}), *P{TRiP.HMS03003}attP40* ($ire1^{RNAi\text{-}1}$), *P{TRiP.HMC05163}attP40* ($ire1^{RNAi\text{-}2}$), *P{TRiP.HMS03015}attP2* ($xbp1^{RNAi\text{-}1}$), *P{TRiP.JF02012}attP2* ($xbp1^{RNAi\text{-}2}$), w^{1118};*PBac{w[+mC] = WH}ire1[f02170]/TM6B,Tb* ($ire1^{f02170}$), *P{TRiP.HMJ02063}attP40* ($perk^{RNAi}$). The following fly lines were obtained from the Tsinghua Fly Center: *P{TRiP.HMS00668} attP2* ($eIF3b^{RNAi}$), *P{TRiP.HMS00762} attP2* ($eIF4G^{RNAi}$), *P{TRiP.HMS02750} attP40* ($atg1^{RNAi}$), *P{TRiP.JF02891} attP2* ($atg9^{RNAi}$), *P{TRiP.HMS01193} attP2* ($atg18^{RNAi}$), *P{TRiP.HMS00551} attP2* ($ref(2)P/p62^{RNAi\text{-}1}$), *P{TRiP.HMS00938} attP2* ($ref(2)P/p62^{RNAi\text{-}2}$), *P{TRiP.HMS00139} attP2* ($pros\beta1^{RNAi}$). The knock-down efficiency of RNAi lines was verified by qPCR. The following flies were maintained in the laboratory of T. Wang: *ATF4-mCherry, ey-flp; FRT82B GMR-hid CL/TM3, ninaE-GFP, trp-GFP, GMR-Gal4, ninaE-xbp1-RE.* All flies were maintained under 12 h light/12 h dark cycles at 25°C unless mentioned.

Generation of transgenic flies

The cDNA sequences of *Rh1, perk, eIF2Bα, atf4*, and *eIF2α* were amplified from RH01460, LD41715, HL01112, RH01327, and GH06180 of the DGRC gold cDNA collections, respectively (*Drosophila* Genomics Resource Center). The *Rh1* cDNA was subcloned into the *pninaE-attB* vector with a C-terminal RFP-tag. $Rh1^{P37H}$ was mutated from the *ninaE* cDNA and subcloned into the *pninaE-attB* vector with a C-terminal GFP-tag. The *perk* cDNA was controlled by its own promotor and subcloned into the *Pperk-attB* vector. The *eIF2Bα* cDNA was subcloned into a *ubi-attB* vector. The *atf4* cDNA was subcloned into a *da-attB* vector. The *eIF2α* cDNA and $eIF2A^{S51A}$ mutated from *eIF2α* cDNA were subcloned into a *pUAST-attB* vector. The *mCherry-T2A-GFP-FLAG-Cl1* sequence was subcloned into the *pninaE-attB* vector. The constructs were injected into *M (vas-int.Dm) ZH-2A;M(3xP3-RFP.attP)ZH-86Fb* or *M (vas-int.Dm) ZH-2A;M (3xP3-RFP.attP) ZH-51C* embryos, and transformants were identified based on eye color. The 3XP3-RFP markers were eliminated by crossing to a Cre-expressing line. To generate the *xbp1-mCherry* reporter flies, the EGFP of *P{UAS-Xbp1.EGFP.HG}* (Ryoo et al., 2007) was replaced by mCherry.

Generation of *atf4*, *atf6*, and *ref(2)P* knockout flies ($atf4^{KO}$, $atf6^{1}$, and $ref(2)P^{m}$)

The $atf4^{KO}$ mutation was generated using the Cas9/sgRNA system (Fig. S4 A; Xu, 2015). Briefly, a pair of guide RNAs targeting the *atf4* locus were designed (sgRNA1: 5′-CTGATTACCAGCTCA ATGAT-3′, sgRNA2: 5′-ACGAGGACTGGGTTCCAGAG-3′) and cloned into the *U6b-sgRNA-short* vector. Plasmids were injected into the embryos of *nos-Cas9* flies, and deletions were identified by PCR using the following primers: forward primer 5′-AAATTG TTTGGCCTCTTTGATG-3′ and reverse primer 5′-TTTTCCTGA TCTTTCGATCCTC-3′.

The $atf6^{1}$ mutation was generated through a combination of sgRNA targeting and *Flp/FRT* recombination as shown in Fig S4 C. Briefly, a pair of guide RNAs targeting the *atf6* locus were designed (sgRNA1: 5′-AATAGAAGGCTCGTGTCGGT-3′, sgRNA2: 5′-TCTTGTTGTACAGTATTGAC-3′) and cloned into the *U6b-sgRNA-short* vector. A pair of homology arm (800 bp upstream and 800 bp downstream of each sgRNA site) sequences were

cloned into the 5′ and 3′ ends of a FRT sequence (5′-GAAGTT CCTATACTTTCTAGAGAATAGGAACTTC-3′). The two pairs of sgDNA and FRT constructs were injected into the embryos of *nos-Cas9* flies, and the flies with both FRT sites replaced were identified by PCR using the following primers: FRT-up: 5′-CAA TAGAAGGGAAGTTCCTATA-3′; FRT-down: 5′-CTGTCACATACC TGAAGTTCCT-3′.

The $atf6^{FRT}$ knock-in flies, were cross with *hs-flp* lines to delete the DNA fragments between the two *FRT* sites. The following PCR primers were used to verify the $atf6^{1}$ flies: ATF6-FRT del-F: 5′-CGCTAACCTCAATACGAAATGG-3′; ATF6-FRT del-R: 5′-TTCATACGGACAGACGGACATA-3′.

The $ref(2)P^{m}$ mutation was generated using a single guide DNA (sgDNA: 5′-ACTGAGTCAAGACTCCGGCA-3′). The plasmid was injected into *nos-Cas9* embryos. A mutant allele in which 4 nucleotides were deleted was identified by PCR and DNA sequencing using the following primers: 5′-f-GAGCCCTCAGTG ATTCACCT-3′ and 5′-r-CTGGATTGACCCTGCTCTTCT-3′. All mutant flies generated were backcrossed to wild-type flies (w^{1118}) before preforming experiment.

EMS mutagenesis

The second chromosome of *FRT40A;*$Rh1^{P37H}$*-GFP* or *FRT42D;* $Rh1^{P37H}$*-GFP* flies and the third chromosome of *FRT2A* $Rh1^{P37H}$*-GFP* or *FTR82B* $Rh1^{P37H}$*-GFP* flies were isogenized, and young male flies were fed 25 mM EMS (Sigma-Aldrich) in 2% sucrose for 8 h, followed by mating to *ey-flp Rh1-RFP;FRT40A GMR-hid CL/Cyo, ey-flp Rh1-RFP;FRT42D GMR-hid CL/Cyo, ey-flp Rh1-RFP; FRT2A GMR-hid CL/TM3* and *ey-flp Rh1-RFP;FRT82B GMR-hid CL/ TM3* flies, respectively. Approximately 100,000 F1 progeny for each chromosomal arm were examined for fluorescence of GFP-tagged $Rh1^{P37H}$ and RFP-tagged wild-type Rh1 (Fig S2A).

Fly imaging

Flies were anaesthetized by CO_2, and fluorescence images were taken with a Leica M165 FC Fluorescent Stereo Microscope.

Immunoprecipitation and Western blots

Approximately 200 fly heads were lysed with 10 mM Tris-HCl lysis buffer (10 mM Tris/Cl pH 7.5; 150 mM NaCl; 0.5 mM EDTA; 0.5% NP-40, 0.09% Na-Azide with 1× proteinase inhibitor cocktail [Roche] and 1 mM PMSF) for 30 min, and centrifuged at 20,000 *g*. The supernatant was used for subsequent immunoprecipitation with anti-GFP beads (Chromotek). Beads were washed in ice-cold dilution buffer (10 mM Tris/Cl pH 7.5; 150 mM NaCl; 0.5 mM EDTA, 0.018% Na-Azide with 1× proteinase inhibitor cocktail and 1 mM PMSF) three times and boiled (45°C, 700 rpm, 30 min) in SDS loading buffer for standard Western blot assays.

For Western blot assays, dissected adult fly heads were homogenized with a pellet pestle (Thermo Fisher Scientific) in SDS loading buffer for SDS-PAGE. The blots were probed with primary antibodies against Rh1 (mouse, 1:2,000; Developmental Studies Hybridoma Bank), INAD (rat, 1:2,000; Wang et al., 2008), mouse anti-β-actin (1:2,000; Santa Cruz), mouse anti-ubiquitin (1:1,000; Santa Cruz), rabbit anti-GFP (1:3,000; easybio), tubulin (mouse, 1:2,000; Developmental Studies Hybridoma Bank), RFP (rabbit, 1:2,000; Biovision), TRP (rabbit, 1:2,000; Wang et al., 2008), Flag (mouse, 1:2,000; Sigma-Aldrich), Ref(2)P/P62 (rabbit, 1:2,000; Abmart), followed by incubation with IRDye 680 goat anti-mouse IgG (1:10,000; LI-COR Biosciences), IRDye 800 goat anti-rabbit IgG (1:10,000, LI-COR Biosciences), or IRDye 680 goat anti-rat IgG (1:10,000; LI-COR Biosciences). Signals were detected using an Odyssey infrared imaging system (LI-COR Biosciences).

Immunostaining

Fly heads were cut and fixed in 4% freshly made paraformaldehyde (Sigma-Aldrich) in phosphate buffer for 2 h on ice, then the retinas were dissected for immunostaining. Samples were incubated with primary antibodies including mouse anti-Rh1 (1:200; Developmental Studies Hybridoma Bank), rat anti–INAD (1:200; Wang et al., 2008), rat anti–RFP antibody (1:200; Chromotek), rabbit anti-Ref(2)P/P62 (1:200; Abmart), rabbit anti-calnexin (1:200; Zhao and Wang, 2020), rabbit anti-Atg8a (1:200; Abcam) at 4 °C overnight, followed by incubation with Alexa Fluor 488–conjugated, Alexa Fluor 568–conjugated, Alexa Fluor 647–conjugated secondary antibodies (1:500; Invitrogen), and 20 nM DAPI (Invitrogen) or phalloidin (Invitrogen) for 1 h at room temperature. Fluorescence images were acquired at room temperature using a LSM800 confocal laser scanning microscope (Zeiss) with a 63×/1.4-NA oil-immersion lens or a 40×/0.95-NA dry lens and Zeiss Application Suite ZEN software (Zeiss Microsystems).

ERG recordings

ERG recordings were performed as described (Wang et al., 2008). Briefly, two glass microelectrodes filled with Ringer's solution were placed on small drops of electrode cream (Parker Laboratories) on the compound eye and the thorax of a fly. For PDA recordings, flies were dark adapted for 2 min. White-eyed flies were then exposed to 5 s of orange light, followed by two rounds of 5 s of blue light, and two rounds of 5 s of orange light. The time between two stimulations was 5 s. For the summed light responses of photoreceptor cells, flies were dark adapted for 2 min and then white-eyed flies were exposed to a 1-s pulse of ∼2,000 lux orange light (source light was filtered using an FSR-OG550 filter, Newport). ERG signals were amplified with a Warner electrometer IE-210 and recorded with a MacLab/4 s analog-to-digital converter and the clampelx 10.2 program (Warner Instruments). All recordings were carried out at room temperature.

Transmission electron microscopy

TEM was performed with standard methods as described (Xu and Wang, 2016). Briefly, fly heads were cut and fixed in 4% paraformaldehyde and 2.5% glutaraldehyde at 4°C overnight followed by incubation in 1% osmium tetroxide for 1–2 h at 4°C. Then the samples were dehydrated using a series of ethanol dilutions (10, 25, 35, 40, 55, 70, 85, 95, and 100% ethanol) and embedded in LR White resin (Polysciences, Inc.). Thin sections (80 nm) were stained with uranyl acetate and lead citrate (Sigma-Aldrich) and examined using a JEOL JEM-1400 transmission electron microscope (JEOL Ltd.) at room temperature. The images were acquired using a Gatan CCD (4 k × 3.7 k pixels).

RNA extraction and quantitative real-time PCR analysis

Fly eyes were dissected, and RNA was extracted using TRIzol Reagent (Invitrogen). Total RNA was reverse-transcribed using EasyScript All-in-One First-Strand cDNA Synthesis SuperMix for qPCR (TransGen). qRT-PCR was performed using iTaq Universal SYBR Green Supermix (BIO-RAD) on a CFX96 real time PCR detection system (Bio-Rad). The average threshold cycle value (CT) was calculated from at least three replicates per sample. Expression of genes were standardized relative to *rp49*. Relative expression values were determined by the ΔΔ CT method. Primers used as below.

rp49-F: 5′-AGCATACAGGCCCAAGATCG-3′, *rp49-R*: 5′-TGTTGTCGATACCCTTGGGC-3′
Hsc70-3-F: 5′-GGTAACCGCATCACTCCCTC-3′, *Hsc70-3-R*: 5′-GTGGTCAACTGATTCTTGGCG-3′
BI-1-F: 5′-GCCACTCTAGTCCTGGTCTTG-3′, *BI-1-R*: 5′-GCCGGAGCAGAATCCGAAG-3′
Gp93-F: 5′-ATCCGCCTATTGGCTCTGTC-3′, *Gp93-R*: 5′-CCGAGTCCATGATGTGCAAC-3′
CaBP1-F: 5′-GAGGTGCTGAAAGACGACG-3′, *CaBP1-R*: 5′-CGACTCCCTTCAATGCCTTGG-3′
Ero1L-F: 5′-CTTCTTCCGCTTCTACAAGGTG-3′, *Ero1L-R*: 5′-CTTGATGCCCTGGGGAATCG-3′
Sec22-F: 5′-GGACGCAGCATACTGGACTAC-3′, *Sec22-R*: 5′-GTCCGGTCTCGATACTGCATC-3′
atg1-F: 5′-CGTCAGCCTGGTCATGGAGTA-3′, *atg1-R*: 5′-TAACGGTATCCTCGCTGAG-3′
atg2-F: 5′-ATGCGCTGATGACCAACGA-3′, *atg2-R*: 5′-CCGACGACCACATGGACTC-3′
atg3-F: 5′-TCAATGTGGCCGAATATCTGAC-3′, *atg3-R*: 5′-AGGTAGGGTTTTGTCTTGGTCT-3′
atg8a-F: 5′-GGTCAGTTCTACTTCCTCATTCG-3′, *atg8a-R*: 5′-GATGTTCCTGGTACAGGGAGC-3′
atg9-F: 5′-TCTAGCCCACATATCAACTACCG-3′, *atg9-R*: 5′-CTTTTGCGTCTTGTGTTTTGGAT-3′
atg18a-F: 5′-ACCACACGAAAAGCGACGAG-3′, *atg18a-R*: 5′-5′-GCTCTGCTTCTTAAAGTGGCAC-3′
perk-F: 5′-TACTAGGTCCAGTGGTGC-3′, *perk-R*: 5′-GCTTGTCCAGGTGGGAAGCTA-3′
ire1-F: 5′-ACTTCGCGGGCCATCTATCTA-3′, *ire1-R*: 5′-GCACTCACAGCATTGTAGTCGTA-3′
eIF3B-F: 5′-GGATGCGAACGACAGTGATTA-3′, *eIF3B-R*: 5′-GGGATATTGTCCACTACCACCA-3′
prosβ1-F: 5′-GGTCATTGGAGCCGATTCG-3′, *prosβ1-R*: 5′-GCAGTACACTTTGTCCGTGAT-3′
xbp1-F: 5′-CCGAACTGAAGCAGCAACAGC-3′, *xbp1-R*: 5′-CAGAGGGTCAGCTTTGGATGC-3′
xbp1-splicing-F: 5′-CCGAACTGAAGCAGCAACAGC-3′,
xbp1-splicing-R: 5′-ATACCCTGCGGCAGATCCAA-3′
ref(2)P/p62-F: 5′-AATCGAGCTGTATCTTTTCCAGG-3′,
ref(2)P/p62-R: 5′-AACGTGCATATTGCTCTCGCA-3′
eIF4G-F: 5′-TATAACCCACGGCAACAAACAT-3′,
eIF4G-R: 5′-TGCTGAAGAGTTGGGACATATTG-3′.

RNA sequencing

RNA sequencing (RNA-seq) assays were performed to analyze the transcriptome of fly retinas. Briefly, 20 retinas were dissected from 1-d-old flies. Total RNA was purified using Trizol reagent. RNA integrity was checked using a 2,100 Bioanalyzer (Agilent Technologies) with a minimum RNA integrity number of 8. The mRNA was enriched using oligo magnetic beads (Invitrogen) and fragmented to ∼150–250 bp. cDNAs were synthesized using random hexamer primers and purified using a MinElute PCR purification kit (Qiagen). The 42-cycle single-end sequencing was performed using an Illumina Genome Analyzer IIx. CASAVA pipeline v1.8 was then used for sequence extraction and filtering. RNA-seq reads were mapped to the fly genome using Tophat (v2.0.8b) software and the Ensembl genome annotation dataset (*Drosophila_melanogaster*.BDGP5.71.gtf). Gene expression level fragments per kilobase of exon per million fragments mapped (FPKM) was estimated using Cufflinks (v2.1.1) software.

Proteomic analysis of the fly retina

40 retina pairs for each genotype (1-d-old) were dissected in cold phosphate buffer. Two samples were generated for each genotype. Protein extraction was performed as described using 50 µl lysis buffer (10% SDS with 100 mM TEAB) for 30 mins on ice and centrifuged at 16,000 *g* to collect supernatant (Xiong et al., 2020). About 50 µg protein for each sample was collected and digested with trypsin (Promega Corporation) in an enzyme/protein ratio of 1:50 (w/w) overnight at 37°C. The resulting peptide samples were labeled using the TMT 10plex Isobaric Label Reagent Set label kit (Thermo). The mixed peptides were fractionated using a reversed phase C18 column (3 M, Bracknell), and 8 fractions of peptide were eluted with acetonitrile step gradients (7.5, 10, 12.5, 15, 17.5, 20, 22.5, and 50%, pH 10). Finally, the eight fractions were dried in a vacuum centrifuge and stored at −80°C until LCMS/MS analysis.

Approximately 2 µg of each pH fractionated peptide sample were separated on an in-house packed 75-µm ID × 50 cm capillary column with 2.5 µm Venusil C18 beads (Agela Technologies) using an EASY-nLC 1,000 system (Thermo Fisher Scientific) with flow rate at 200 nl/min. Raw data was collected on Q Exactive mass spectrometer (Thermo Fisher Scientific) using Thermo Xcalibur (2.0) software. All raw LC–MS/MS data were submitted to Proteome Discoverer (2.2 version, Thermo Science) for TMT quantitation and database analysis using SequestHT. Data were searched against the Fruit fly Swiss-Prot database (UP000000803, 21,922 sequences) in combination with a common contaminants database (247 entries).

Statistics

Statistical results were generated by GraphPad Prism 6 and statistical significance was assessed through Ordinary one/two-way ANOVA, Sidak's multiple comparisons test, and Student's *t* test analyses. All error bars represent standard error of the mean. ImageJ was used to quantify the fluorescence intensity of Western blot and immunostaining images. A graphical normality test was performed to determine whether all data used for statistical analysis were normally distributed. Briefly, a histogram of the dataset was created, and all data fall in a normally distributed population.

Online supplemental material

Fig. S1 shows that a genetic screen reveals that *perk* and *eIF2Bα* are involved in Rh1 homeostasis in a model of adRP. Fig. S2 shows the levels of $Rh1^{P37H}$ and endogenous Rh1 are unaffected by mutations in *ire1* and *atf6*. Fig. S3 shows the overlap of upregulated genes in $Rh1^{P37H}$*-GFP* $perk^{RNAi}$ and *ninaE-xbp1-RE* retinas. Fig. S4 shows that the ER proteins are degraded through autophagy in $Rh1^{P37H}$*-GFP* $perk^{RNAi}$ photoreceptor cells. Fig. S5 shows that the ER-phagy is induced in the $ninaE^{G69D}$ model of adRP. Data S1 shows the gene expression profiling of retina of the $Rh1^{P37H}$*-GFP* $perk^{RNAi}$ and $Rh1^{P37H}$*-GFP* flies related to Fig. 4 A. Data S2 shows the gene expression profiling of retina dissected from the *ninaE-GFP* and *ninaE-xbp1-RE* flies related to Fig. S3 A. Data S3 shows comparison of retinal protein levels of $Rh1^{P37H}$*-GFP* $perk^{RNAi}$ with $Rh1^{P37H}$*-GFP* flies related to Fig. 5 A.

Data availability

All data are available in the main text or the supplementary materials.

Acknowledgments

We thank the Bloomington Stock Center, the *Drosophila* Genomic Resource Center, the Tsinghua Fly Center, and the Developmental Studies Hybridoma Bank for stocks and reagents. We thank Y. Wang and X. Liu for assistance with fly injections. We are tremendously thankful for support provided by the Sequencing Center, the Electron Microscopy Center, the Imaging Facility, and the Proteomics Facility at the National Institute of Biological Sciences. We thank Dr. Lin Yang from the Institute of Genetics and Developmental Biology for assistance with TEM. We thank Dr. D. O'Keefe for editing the manuscript.

This work was supported by grants from the National Natural Science Foundation of China (81870693 and 81670891) awarded to T. Wang.

Author contributions: Methodology: T. Wang, N. Zhao. Investigation: N. Zhao. Visualization: N. Zhao, N. Li. Supervision: TW. Writing—original draft: T. Wang, N. Zhao. Writing—review & editing: T. Wang, N. Zhao.

Disclosures: The authors declare no competing interests exist.

Submitted: 26 August 2022
Revised: 4 January 2023
Accepted: 14 February 2023

References

Adomavicius, T., M. Guaita, Y. Zhou, M.D. Jennings, Z. Latif, A.M. Roseman, and G.D. Pavitt. 2019. The structural basis of translational control by eIF2 phosphorylation. *Nat. Commun.* 10:2136. https://doi.org/10.1038/s41467-019-10167-3

An, H., A. Ordureau, J.A. Paulo, C.J. Shoemaker, V. Denic, and J.W. Harper. 2019. TEX264 is an endoplasmic reticulum-resident ATG8-interacting protein critical for ER remodeling during nutrient stress. *Mol. Cell.* 74: 891–908.e10. https://doi.org/10.1016/j.molcel.2019.03.034

Andreev, D.E., P.B. O'Connor, C. Fahey, E.M. Kenny, I.M. Terenin, S.E. Dmitriev, P. Cormican, D.W. Morris, I.N. Shatsky, and P.V. Baranov. 2015. Translation of 5′ leaders is pervasive in genes resistant to eIF2 repression. *Elife.* 4:e03971. https://doi.org/10.7554/eLife.03971

Athanasiou, D., M. Aguila, J. Bellingham, N. Kanuga, P. Adamson, and M.E. Cheetham. 2017. The role of the ER stress-response protein PERK in rhodopsin retinitis pigmentosa. *Hum. Mol. Genet.* 26:4896–4905. https://doi.org/10.1093/hmg/ddx370

Athanasiou, D., M. Aguila, J. Bellingham, W. Li, C. McCulley, P.J. Reeves, and M.E. Cheetham. 2018. The molecular and cellular basis of rhodopsin retinitis pigmentosa reveals potential strategies for therapy. *Prog. Retin. Eye Res.* 62:1–23. https://doi.org/10.1016/j.preteyeres.2017.10.002

B'chir, W., A.C. Maurin, V. Carraro, J. Averous, C. Jousse, Y. Muranishi, L. Parry, G. Stepien, P. Fafournoux, and A. Bruhat. 2013. The eIF2α/ATF4 pathway is essential for stress-induced autophagy gene expression. *Nucleic Acids Res.* 41:7683–7699. https://doi.org/10.1093/nar/gkt563

Baird, T.D., L.R. Palam, M.E. Fusakio, J.A. Willy, C.M. Davis, J.N. McClintick, T.G. Anthony, and R.C. Wek. 2014. Selective mRNA translation during eIF2 phosphorylation induces expression of IBTKα. *Mol. Biol. Cell.* 25: 1686–1697. https://doi.org/10.1091/mbc.e14-02-0704

Berry, D.L., and E.H. Baehrecke. 2007. Growth arrest and autophagy are required for salivary gland cell degradation in Drosophila. *Cell.* 131: 1137–1148. https://doi.org/10.1016/j.cell.2007.10.048

Bhattacharjee, A., A. Ürmösi, A. Jipa, L. Kovács, P. Deák, Á. Szabó, and G. Juhász. 2022. Loss of ubiquitinated protein autophagy is compensated by persistent cnc/NFE2L2/Nrf2 antioxidant responses. *Autophagy.* 18: 2385–2396. https://doi.org/10.1080/15548627.2022.2037852

Bhootada, Y., P. Kotla, S. Zolotukhin, O. Gorbatyuk, Z. Bebok, M. Athar, and M. Gorbatyuk. 2016. Limited ATF4 expression in degenerating retinas with ongoing ER stress promotes photoreceptor survival in a mouse model of autosomal dominant retinitis pigmentosa. *PLoS One.* 11: e0154779. https://doi.org/10.1371/journal.pone.0154779

Brown, B., S. Mitra, F.D. Roach, D. Vasudevan, and H.D. Ryoo. 2021. The transcription factor Xrp1 is required for PERK-mediated antioxidant gene induction in *Drosophila*. *Elife.* 10:e74047. https://doi.org/10.7554/eLife.74047

Calfon, M., H. Zeng, F. Urano, J.H. Till, S.R. Hubbard, H.P. Harding, S.G. Clark, and D. Ron. 2002. IRE1 couples endoplasmic reticulum load to secretory capacity by processing the XBP-1 mRNA. *Nature.* 415:92–96. https://doi.org/10.1038/415092a

Celardo, I., A.C. Costa, S. Lehmann, C. Jones, N. Wood, N.E. Mencacci, G.R. Mallucci, S.H. Loh, and L.M. Martins. 2016. Mitofusin-mediated ER stress triggers neurodegeneration in pink1/parkin models of Parkinson's disease. *Cell Death Dis.* 7:e2271. https://doi.org/10.1038/cddis.2016.173

Chang, T.K., D.A. Lawrence, M. Lu, J. Tan, J.M. Harnoss, S.A. Marsters, P. Liu, W. Sandoval, S.E. Martin, and A. Ashkenazi. 2018. Coordination between two branches of the unfolded protein response determines apoptotic cell fate. *Mol. Cell.* 71:629–636.e5. https://doi.org/10.1016/j.molcel.2018.06.038

Chen, Q., Y. Xiao, P. Chai, P. Zheng, J. Teng, and J. Chen. 2019. ATL3 is a tubular ER-phagy receptor for GABARAP-mediated selective autophagy. *Curr. Biol.* 29:846–855.e6. https://doi.org/10.1016/j.cub.2019.01.041

Chiang, W.C., N. Hiramatsu, C. Messah, H. Kroeger, and J.H. Lin. 2012a. Selective activation of ATF6 and PERK endoplasmic reticulum stress signaling pathways prevent mutant rhodopsin accumulation. *Invest. Ophthalmol. Vis. Sci.* 53:7159–7166. https://doi.org/10.1167/iovs.12-10222

Chiang, W.C., H. Kroeger, S. Sakami, C. Messah, D. Yasumura, M.T. Matthes, J.A. Coppinger, K. Palczewski, M.M. LaVail, and J.H. Lin. 2015. Robust endoplasmic reticulum-associated degradation of rhodopsin precedes retinal degeneration. *Mol. Neurobiol.* 52:679–695. https://doi.org/10.1007/s12035-014-8881-8

Chiang, W.C., C. Messah, and J.H. Lin. 2012b. IRE1 directs proteasomal and lysosomal degradation of misfolded rhodopsin. *Mol. Biol. Cell.* 23: 758–770. https://doi.org/10.1091/mbc.e11-08-0663

Coelho, D.S., F. Cairrão, X. Zeng, E. Pires, A.V. Coelho, D. Ron, H.D. Ryoo, and P.M. Domingos. 2013. Xbp1-independent Ire1 signaling is required for photoreceptor differentiation and rhabdomere morphogenesis in Drosophila. *Cell Rep.* 5:791–801. https://doi.org/10.1016/j.celrep.2013.09.046

Colley, N.J., J.A. Cassill, E.K. Baker, and C.S. Zuker. 1995. Defective intracellular transport is the molecular basis of rhodopsin-dependent dominant retinal degeneration. *Proc. Natl. Acad. Sci. USA.* 92:3070–3074. https://doi.org/10.1073/pnas.92.7.3070

Costa-Mattioli, M., and P. Walter. 2020. The integrated stress response: From mechanism to disease. *Science.* 368:368. https://doi.org/10.1126/science.aat5314

Cox, J.S., C.E. Shamu, and P. Walter. 1993. Transcriptional induction of genes encoding endoplasmic reticulum resident proteins requires a transmembrane protein kinase. *Cell.* 73:1197–1206. https://doi.org/10.1016/0092-8674(93)90648-A

Cullinan, S.B., D. Zhang, M. Hannink, E. Arvisais, R.J. Kaufman, and J.A. Diehl. 2003. Nrf2 is a direct PERK substrate and effector of PERK-dependent cell survival. *Mol. Cell. Biol.* 23:7198–7209. https://doi.org/10.1128/MCB.23.20.7198-7209.2003

Doherty, J., and E.H. Baehrecke. 2018. Life, death and autophagy. *Nat. Cell Biol.* 20:1110–1117. https://doi.org/10.1038/s41556-018-0201-5

Dryja, T.P., T.L. McGee, E. Reichel, L.B. Hahn, G.S. Cowley, D.W. Yandell, M.A. Sandberg, and E.L. Berson. 1990. A point mutation of the rhodopsin gene in one form of retinitis pigmentosa. *Nature*. 343:364–366. https://doi.org/10.1038/343364a0

Fawcett, T.W., J.L. Martindale, K.Z. Guyton, T. Hai, and N.J. Holbrook. 1999. Complexes containing activating transcription factor (ATF)/cAMP-responsive-element-binding protein (CREB) interact with the CCAAT/enhancer-binding protein (C/EBP)-ATF composite site to regulate Gadd153 expression during the stress response. *Biochem. J.* 339:135–141. https://doi.org/10.1042/bj3390135

Fumagalli, F., J. Noack, T.J. Bergmann, E. Cebollero, G.B. Pisoni, E. Fasana, I. Fregno, C. Galli, M. Loi, T. Soldà, et al. 2016. Translocon component Sec62 acts in endoplasmic reticulum turnover during stress recovery. *Nat. Cell Biol.* 18:1173–1184. https://doi.org/10.1038/ncb3423

Galy, A., M.J. Roux, J.A. Sahel, T. Léveillard, and A. Giangrande. 2005. Rhodopsin maturation defects induce photoreceptor death by apoptosis: A fly model for RhodopsinPro23His human retinitis pigmentosa. *Hum. Mol. Genet.* 14:2547–2557. https://doi.org/10.1093/hmg/ddi258

Gilon, T., O. Chomsky, and R.G. Kulka. 1998. Degradation signals for ubiquitin system proteolysis in Saccharomyces cerevisiae. *EMBO J.* 17:2759–2766. https://doi.org/10.1093/emboj/17.10.2759

Griciuc, A., L. Aron, M.J. Roux, R. Klein, A. Giangrande, and M. Ueffing. 2010. Inactivation of VCP/ter94 suppresses retinal pathology caused by misfolded rhodopsin in Drosophila. *PLoS Genet.* 6:e1001075. https://doi.org/10.1371/journal.pgen.1001075

Grumati, P., G. Morozzi, S. Hölper, M. Mari, M.I. Harwardt, R. Yan, S. Müller, F. Reggiori, M. Heilemann, and I. Dikic. 2017. Full length RTN3 regulates turnover of tubular endoplasmic reticulum via selective autophagy. *Elife*. 6:e25555. https://doi.org/10.7554/eLife.25555

Hara, T., K. Nakamura, M. Matsui, A. Yamamoto, Y. Nakahara, R. Suzuki-Migishima, M. Yokoyama, K. Mishima, I. Saito, H. Okano, and N. Mizushima. 2006. Suppression of basal autophagy in neural cells causes neurodegenerative disease in mice. *Nature*. 441:885–889. https://doi.org/10.1038/nature04724

Harding, H.P., I. Novoa, Y. Zhang, H. Zeng, R. Wek, M. Schapira, and D. Ron. 2000aa. Regulated translation initiation controls stress-induced gene expression in mammalian cells. *Mol. Cell*. 6:1099–1108. https://doi.org/10.1016/S1097-2765(00)00108-8

Harding, H.P., Y. Zhang, A. Bertolotti, H. Zeng, and D. Ron. 2000bb. Perk is essential for translational regulation and cell survival during the unfolded protein response. *Mol. Cell*. 5:897–904. https://doi.org/10.1016/S1097-2765(00)80330-5

Harding, H.P., Y. Zhang, and D. Ron. 1999. Protein translation and folding are coupled by an endoplasmic-reticulum-resident kinase. *Nature*. 397:271–274. https://doi.org/10.1038/16729

Harding, H.P., Y. Zhang, H. Zeng, I. Novoa, P.D. Lu, M. Calfon, N. Sadri, C. Yun, B. Popko, R. Paules, et al. 2003. An integrated stress response regulates amino acid metabolism and resistance to oxidative stress. *Mol. Cell*. 11:619–633. https://doi.org/10.1016/S1097-2765(03)00105-9

Hartong, D.T., E.L. Berson, and T.P. Dryja. 2006. Retinitis pigmentosa. *Lancet*. 368:1795–1809. https://doi.org/10.1016/S0140-6736(06)69740-7

Haze, K., H. Yoshida, H. Yanagi, T. Yura, and K. Mori. 1999. Mammalian transcription factor ATF6 is synthesized as a transmembrane protein and activated by proteolysis in response to endoplasmic reticulum stress. *Mol. Biol. Cell*. 10:3787–3799. https://doi.org/10.1091/mbc.10.11.3787

He, L., A.S. Kennedy, S. Houck, A. Aleksandrov, N.L. Quinney, A. Cyr-Scully, D.M. Cholon, M. Gentzsch, S.H. Randell, H.Y. Ren, and D.M. Cyr. 2021. DNAJB12 and Hsp70 triage arrested intermediates of N1303K-CFTR for endoplasmic reticulum-associated autophagy. *Mol. Biol. Cell*. 32:538–553. https://doi.org/10.1091/mbc.E20-11-0688

Hetz, C., P. Thielen, S. Matus, M. Nassif, F. Court, R. Kiffin, G. Martinez, A.M. Cuervo, R.H. Brown, and L.H. Glimcher. 2009. XBP-1 deficiency in the nervous system protects against amyotrophic lateral sclerosis by increasing autophagy. *Genes Dev.* 23:2294–2306. https://doi.org/10.1101/gad.1830709

Hetz, C., K. Zhang, and R.J. Kaufman. 2020. Mechanisms, regulation and functions of the unfolded protein response. *Nat. Rev. Mol. Cell Biol.* 21:421–438. https://doi.org/10.1038/s41580-020-0250-z

Hollien, J., and J.S. Weissman. 2006. Decay of endoplasmic reticulum-localized mRNAs during the unfolded protein response. *Science*. 313:104–107. https://doi.org/10.1126/science.1129631

Houck, S.A., H.Y. Ren, V.J. Madden, J.N. Bonner, M.P. Conlin, J.A. Janovick, P.M. Conn, and D.M. Cyr. 2014. Quality control autophagy degrades soluble ERAD-resistant conformers of the misfolded membrane protein GnRHR. *Mol. Cell*. 54:166–179. https://doi.org/10.1016/j.molcel.2014.02.025

Kang, M.J., and H.D. Ryoo. 2009. Suppression of retinal degeneration in Drosophila by stimulation of ER-associated degradation. *Proc. Natl. Acad. Sci. USA*. 106:17043–17048. https://doi.org/10.1073/pnas.0905566106

Kenner, L.R., A.A. Anand, H.C. Nguyen, A.G. Myasnikov, C.J. Klose, L.A. McGeever, J.C. Tsai, L.E. Miller-Vedam, P. Walter, and A. Frost. 2019. eIF2B-catalyzed nucleotide exchange and phosphoregulation by the integrated stress response. *Science*. 364:491–495. https://doi.org/10.1126/science.aaw2922

Khaminets, A., T. Heinrich, M. Mari, P. Grumati, A.K. Huebner, M. Akutsu, L. Liebmann, A. Stolz, S. Nietzsche, N. Koch, et al. 2015. Regulation of endoplasmic reticulum turnover by selective autophagy. *Nature*. 522:354–358. https://doi.org/10.1038/nature14498

Kim, K.H., Y.T. Jeong, S.H. Kim, H.S. Jung, K.S. Park, H.Y. Lee, and M.S. Lee. 2013. Metformin-induced inhibition of the mitochondrial respiratory chain increases FGF21 expression via ATF4 activation. *Biochem. Biophys. Res. Commun.* 440:76–81. https://doi.org/10.1016/j.bbrc.2013.09.026

Klaips, C.L., G.G. Jayaraj, and F.U. Hartl. 2018. Pathways of cellular proteostasis in aging and disease. *J. Cell Biol.* 217:51–63. https://doi.org/10.1083/jcb.201709072

Komatsu, M., S. Waguri, T. Chiba, S. Murata, J. Iwata, I. Tanida, T. Ueno, M. Koike, Y. Uchiyama, E. Kominami, and K. Tanaka. 2006. Loss of autophagy in the central nervous system causes neurodegeneration in mice. *Nature*. 441:880–884. https://doi.org/10.1038/nature04723

Kurada, P., and J.E. O'Tousa. 1995. Retinal degeneration caused by dominant rhodopsin mutations in Drosophila. *Neuron*. 14:571–579. https://doi.org/10.1016/0896-6273(95)90313-5

Kurtishi, A., B. Rosen, K.S. Patil, G.W. Alves, and S.G. Møller. 2019. Cellular proteostasis in neurodegeneration. *Mol. Neurobiol.* 56:3676–3689. https://doi.org/10.1007/s12035-018-1334-z

Lee, E.J., P. Chan, L. Chea, K. Kim, R.J. Kaufman, and J.H. Lin. 2021. ATF6 is required for efficient rhodopsin clearance and retinal homeostasis in the P23H rho retinitis pigmentosa mouse model. *Sci. Rep.* 11:16356. https://doi.org/10.1038/s41598-021-95895-7

Lin, J.H., H. Li, D. Yasumura, H.R. Cohen, C. Zhang, B. Panning, K.M. Shokat, M.M. Lavail, and P. Walter. 2007. IRE1 signaling affects cell fate during the unfolded protein response. *Science*. 318:944–949. https://doi.org/10.1126/science.1146361

Liu, C.Y., M. Schröder, and R.J. Kaufman. 2000. Ligand-independent dimerization activates the stress response kinases IRE1 and PERK in the lumen of the endoplasmic reticulum. *J. Biol. Chem.* 275:24881–24885. https://doi.org/10.1074/jbc.M004454200

Lobanova, E.S., S. Finkelstein, J. Li, A.M. Travis, Y. Hao, M. Klingeborn, N.P. Skiba, R.J. Deshaies, and V.Y. Arshavsky. 2018. Increased proteasomal activity supports photoreceptor survival in inherited retinal degeneration. *Nat. Commun.* 9:1738. https://doi.org/10.1038/s41467-018-04117-8

Lobanova, E.S., S. Finkelstein, N.P. Skiba, and V.Y. Arshavsky. 2013. Proteasome overload is a common stress factor in multiple forms of inherited retinal degeneration. *Proc. Natl. Acad. Sci. USA*. 110:9986–9991. https://doi.org/10.1073/pnas.1305521110

Mendes, H.F., and M.E. Cheetham. 2008. Pharmacological manipulation of gain-of-function and dominant-negative mechanisms in rhodopsin retinitis pigmentosa. *Hum. Mol. Genet.* 17:3043–3054. https://doi.org/10.1093/hmg/ddn202

Mendes, H.F., J. van der Spuy, J.P. Chapple, and M.E. Cheetham. 2005. Mechanisms of cell death in rhodopsin retinitis pigmentosa: Implications for therapy. *Trends Mol. Med.* 11:177–185. https://doi.org/10.1016/j.molmed.2005.02.007

Meusser, B., C. Hirsch, E. Jarosch, and T. Sommer. 2005. Erad: The long road to destruction. *Nat. Cell Biol.* 7:766–772. https://doi.org/10.1038/ncb0805-766

Moore, K., and J. Hollien. 2015. Ire1-mediated decay in mammalian cells relies on mRNA sequence, structure, and translational status. *Mol. Biol. Cell*. 26:2873–2884. https://doi.org/10.1091/mbc.E15-02-0074

Moreno, J.A., M. Halliday, C. Molloy, H. Radford, N. Verity, J.M. Axten, C.A. Ortori, A.E. Willis, P.M. Fischer, D.A. Barrett, and G.R. Mallucci. 2013. Oral treatment targeting the unfolded protein response prevents

neurodegeneration and clinical disease in prion-infected mice. *Sci. Transl. Med.* 5:206ra138. https://doi.org/10.1126/scitranslmed.3006767

Mori, K., W. Ma, M.J. Gething, and J. Sambrook. 1993. A transmembrane protein with a cdc2+/CDC28-related kinase activity is required for signaling from the ER to the nucleus. *Cell*. 74:743–756. https://doi.org/10.1016/0092-8674(93)90521-Q

Moscat, J., and M.T. Diaz-Meco. 2012. p62: A versatile multitasker takes on cancer. *Trends Biochem. Sci.* 37:230–236. https://doi.org/10.1016/j.tibs.2012.02.008

Nagy, P., A. Varga, K. Pircs, K. Hegedűs, and G. Juhász. 2013. Myc-driven overgrowth requires unfolded protein response-mediated induction of autophagy and antioxidant responses in Drosophila melanogaster. *PLoS Genet.* 9:e1003664. https://doi.org/10.1371/journal.pgen.1003664

Nezis, I.P., A. Simonsen, A.P. Sagona, K. Finley, S. Gaumer, D. Contamine, T.E. Rusten, H. Stenmark, and A. Brech. 2008. Ref(2)P, the Drosophila melanogaster homologue of mammalian p62, is required for the formation of protein aggregates in adult brain. *J. Cell Biol.* 180:1065–1071. https://doi.org/10.1083/jcb.200711108

Nonaka, T., and M. Hasegawa. 2009. A cellular model to monitor proteasome dysfunction by α-synuclein. *Biochemistry*. 48:8014–8022. https://doi.org/10.1021/bi900619j

O'Tousa, J.E., W. Baehr, R.L. Martin, J. Hirsh, W.L. Pak, and M.L. Applebury. 1985. The Drosophila ninaE gene encodes an opsin. *Cell*. 40:839–850. https://doi.org/10.1016/0092-8674(85)90343-5

Ogata, M., S. Hino, A. Saito, K. Morikawa, S. Kondo, S. Kanemoto, T. Murakami, M. Taniguchi, I. Tanii, K. Yoshinaga, et al. 2006. Autophagy is activated for cell survival after endoplasmic reticulum stress. *Mol. Cell. Biol.* 26:9220–9231. https://doi.org/10.1128/MCB.01453-06

Princely Abudu, Y., S. Pankiv, B.J. Mathai, A. Håkon Lystad, C. Bindesbøll, H.B. Brenne, M. Yoke Wui Ng, B. Thiede, A. Yamamoto, T. Mutugi Nthiga, et al. 2019. NIPSNAP1 and NIPSNAP2 act as "eat me" signals for mitophagy. *Dev. Cell*. 49:509–525.e12. https://doi.org/10.1016/j.devcel.2019.03.013

Qiu, Y., J. Yao, L. Jia, D.A. Thompson, and D.N. Zacks. 2019. Shifting the balance of autophagy and proteasome activation reduces proteotoxic cell death: A novel therapeutic approach for restoring photoreceptor homeostasis. *Cell Death Dis.* 10:547. https://doi.org/10.1038/s41419-019-1780-1

Rajan, R.S., and R.R. Kopito. 2005. Suppression of wild-type rhodopsin maturation by mutants linked to autosomal dominant retinitis pigmentosa. *J. Biol. Chem.* 280:1284–1291. https://doi.org/10.1074/jbc.M406448200

Rosenbaum, E.E., E. Vasiljevic, K.S. Brehm, and N.J. Colley. 2014. Mutations in four glycosyl hydrolases reveal a highly coordinated pathway for rhodopsin biosynthesis and N-glycan trimming in Drosophila melanogaster. *PLoS Genet.* 10:e1004349. https://doi.org/10.1371/journal.pgen.1004349

Ryoo, H.D., P.M. Domingos, M.J. Kang, and H. Steller. 2007. Unfolded protein response in a Drosophila model for retinal degeneration. *EMBO J.* 26:242–252. https://doi.org/10.1038/sj.emboj.7601477

Sakami, S., T. Maeda, G. Bereta, K. Okano, M. Golczak, A. Sumaroka, A.J. Roman, A.V. Cideciyan, S.G. Jacobson, and K. Palczewski. 2011. Probing mechanisms of photoreceptor degeneration in a new mouse model of the common form of autosomal dominant retinitis pigmentosa due to P23H opsin mutations. *J. Biol. Chem.* 286:10551–10567. https://doi.org/10.1074/jbc.M110.209759

Saliba, R.S., P.M. Munro, P.J. Luthert, and M.E. Cheetham. 2002. The cellular fate of mutant rhodopsin: Quality control, degradation and aggresome formation. *J. Cell Sci.* 115:2907–2918. https://doi.org/10.1242/jcs.115.14.2907

Sano, R., and J.C. Reed. 2013. ER stress-induced cell death mechanisms. *Biochim. Biophys. Acta*. 1833:3460–3470. https://doi.org/10.1016/j.bbamcr.2013.06.028

Scapin, C., C. Ferri, E. Pettinato, F. Bianchi, U. Del Carro, M.L. Feltri, R.J. Kaufman, L. Wrabetz, and M. D'Antonio. 2020. Phosphorylation of eIF2α promotes schwann cell differentiation and myelination in CMT1B mice with activated UPR. *J. Neurosci.* 40:8174–8187. https://doi.org/10.1523/JNEUROSCI.0957-20.2020

Shamu, C.E., and P. Walter. 1996. Oligomerization and phosphorylation of the Ire1p kinase during intracellular signaling from the endoplasmic reticulum to the nucleus. *EMBO J.* 15:3028–3039. https://doi.org/10.1002/j.1460-2075.1996.tb00666.x

Shen, J., X. Chen, L. Hendershot, and R. Prywes. 2002. ER stress regulation of ATF6 localization by dissociation of BiP/GRP78 binding and unmasking of Golgi localization signals. *Dev. Cell*. 3:99–111. https://doi.org/10.1016/S1534-5807(02)00203-4

Shi, Y., K.M. Vattem, R. Sood, J. An, J. Liang, L. Stramm, and R.C. Wek. 1998. Identification and characterization of pancreatic eukaryotic initiation factor 2 α-subunit kinase, PEK, involved in translational control. *Mol. Cell. Biol.* 18:7499–7509. https://doi.org/10.1128/MCB.18.12.7499

Shoulders, M.D., L.M. Ryno, J.C. Genereux, J.J. Moresco, P.G. Tu, C. Wu, J.R. Yates III, A.I. Su, J.W. Kelly, and R.L. Wiseman. 2013. Stress-independent activation of XBP1s and/or ATF6 reveals three functionally diverse ER proteostasis environments. *Cell Rep.* 3:1279–1292. https://doi.org/10.1016/j.celrep.2013.03.024

Vasudevan, D., H. Katow, H.W. Huang, G. Tang, and H.D. Ryoo. 2022. A protein-trap allele reveals roles for Drosophila ATF4 in photoreceptor degeneration, oogenesis and wing development. *Dis. Model. Mech.* 15:dmm049119. https://doi.org/10.1242/dmm.049119

Vasudevan, D., S.D. Neuman, A. Yang, L. Lough, B. Brown, A. Bashirullah, T. Cardozo, and H.D. Ryoo. 2020. Translational induction of ATF4 during integrated stress response requires noncanonical initiation factors eIF2D and DENR. *Nat. Commun.* 11:4677. https://doi.org/10.1038/s41467-020-18453-1

Vembar, S.S., and J.L. Brodsky. 2008. One step at a time: Endoplasmic reticulum-associated degradation. *Nat. Rev. Mol. Cell Biol.* 9:944–957. https://doi.org/10.1038/nrm2546

Vidal, R.L., A. Figueroa, F.A. Court, P. Thielen, C. Molina, C. Wirth, B. Caballero, R. Kiffin, J. Segura-Aguilar, A.M. Cuervo, et al. 2012. Targeting the UPR transcription factor XBP1 protects against Huntington's disease through the regulation of FoxO1 and autophagy. *Hum. Mol. Genet.* 21:2245–2262. https://doi.org/10.1093/hmg/dds040

Walter, P., and D. Ron. 2011. The unfolded protein response: From stress pathway to homeostatic regulation. *Science*. 334:1081–1086. https://doi.org/10.1126/science.1209038

Wang, T., U. Lao, and B.A. Edgar. 2009. TOR-mediated autophagy regulates cell death in Drosophila neurodegenerative disease. *J. Cell Biol.* 186:703–711. https://doi.org/10.1083/jcb.200904090

Wang, T., and C. Montell. 2007. Phototransduction and retinal degeneration in Drosophila. *Pflugers Arch.* 454:821–847. https://doi.org/10.1007/s00424-007-0251-1

Wang, T., X. Wang, Q. Xie, and C. Montell. 2008. The SOCS box protein STOPS is required for phototransduction through its effects on phospholipase C. *Neuron*. 57:56–68. https://doi.org/10.1016/j.neuron.2007.11.020

Wang, Y., C. Punzo, J.D. Ash, and E.S. Lobanova. 2022. Tsc2 knockout counteracts ubiquitin-proteasome system insufficiency and delays photoreceptor loss in retinitis pigmentosa. *Proc. Natl. Acad. Sci. USA*. 119:e2118479119. https://doi.org/10.1073/pnas.2118479119

Wei, Y., W.C. Chiang, R. Sumpter Jr, P. Mishra, and B. Levine. 2017. Prohibitin 2 is an inner mitochondrial membrane mitophagy receptor. *Cell*. 168:224–238.e10. https://doi.org/10.1016/j.cell.2016.11.042

Xiong, L., L. Zhang, Y. Yang, N. Li, W. Lai, F. Wang, X. Zhu, and T. Wang. 2020. ER complex proteins are required for rhodopsin biosynthesis and photoreceptor survival in Drosophila and mice. *Cell Death Differ.* 27:646–661. https://doi.org/10.1038/s41418-019-0378-6

Xu, Y., et al. 2015. Histamine Recycling Is Mediated by CarT, a Carcinine Transporter in *Drosophila* Photoreceptors. *PLoS Genetics*. 11. https://doi.org/10.1371/journal.pgen.1005764

Xu, Y., and T. Wang. 2016. CULD is required for rhodopsin and TRPL channel endocytic trafficking and survival of photoreceptor cells. *J. Cell Sci.* 129:394–405. https://doi.org/10.1242/jcs.178764

Xu, J., H. Zhao, and T. Wang. 2020. Suppression of retinal degeneration by two novel ERAD ubiquitin E3 ligases SORDD1/2 in Drosophila. *PLoS Genet.* 16:e1009172. https://doi.org/10.1371/journal.pgen.1009172

Yan, C., J. Liu, J. Gao, Y. Sun, L. Zhang, H. Song, L. Xue, L. Zhan, G. Gao, Z. Ke, et al. 2019. IRE1 promotes neurodegeneration through autophagy-dependent neuron death in the Drosophila model of Parkinson's disease. *Cell Death Dis.* 10:800. https://doi.org/10.1038/s41419-019-2039-6

Yao, J., Y. Qiu, E. Frontera, L. Jia, N.W. Khan, D.J. Klionsky, T.A. Ferguson, D.A. Thompson, and D.N. Zacks. 2018. Inhibiting autophagy reduces retinal degeneration caused by protein misfolding. *Autophagy*. 14:1226–1238. https://doi.org/10.1080/15548627.2018.1463121

Yorimitsu, T., U. Nair, Z. Yang, and D.J. Klionsky. 2006. Endoplasmic reticulum stress triggers autophagy. *J. Biol. Chem.* 281:30299–30304. https://doi.org/10.1074/jbc.M607007200

Yoshida, H., T. Matsui, A. Yamamoto, T. Okada, and K. Mori. 2001. XBP1 mRNA is induced by ATF6 and spliced by IRE1 in response to ER stress to produce a highly active transcription factor. *Cell*. 107:881–891. https://doi.org/10.1016/S0092-8674(01)00611-0

Zhang, W., V. Hietakangas, S. Wee, S.C. Lim, J. Gunaratne, and S.M. Cohen. 2013. ER stress potentiates insulin resistance through PERK-mediated

FOXO phosphorylation. *Genes Dev.* 27:441–449. https://doi.org/10.1101/gad.201731.112

Zhao, H., J. Wang, and T. Wang. 2018. The V-ATPase V1 subunit A1 is required for rhodopsin anterograde trafficking in Drosophila. *Mol. Biol. Cell.* 29: 1640–1651. https://doi.org/10.1091/mbc.E17-09-0546

Zhao, H., and T. Wang. 2020. PE homeostasis rebalanced through mitochondria-ER lipid exchange prevents retinal degeneration in Drosophila. *PLoS Genet.* 16:e1009070. https://doi.org/10.1371/journal.pgen.1009070

Zhou, D., L.R. Palam, L. Jiang, J. Narasimhan, K.A. Staschke, and R.C. Wek. 2008. Phosphorylation of eIF2 directs ATF5 translational control in response to diverse stress conditions. *J. Biol. Chem.* 283:7064–7073. https://doi.org/10.1074/jbc.M708530200

Zhu, H., B. Bhatt, S. Sivaprakasam, Y. Cai, S. Liu, S.K. Kodeboyina, N. Patel, N.M. Savage, A. Sharma, R.J. Kaufman, et al. 2019. Ufbp1 promotes plasma cell development and ER expansion by modulating distinct branches of UPR. *Nat. Commun.* 10:1084. https://doi.org/10.1038/s41467-019-08908-5

Zuker, C.S., A.F. Cowman, and G.M. Rubin. 1985. Isolation and structure of a rhodopsin gene from D. melanogaster. *Cell.* 40:851–858. https://doi.org/10.1016/0092-8674(85)90344-7

Supplemental material

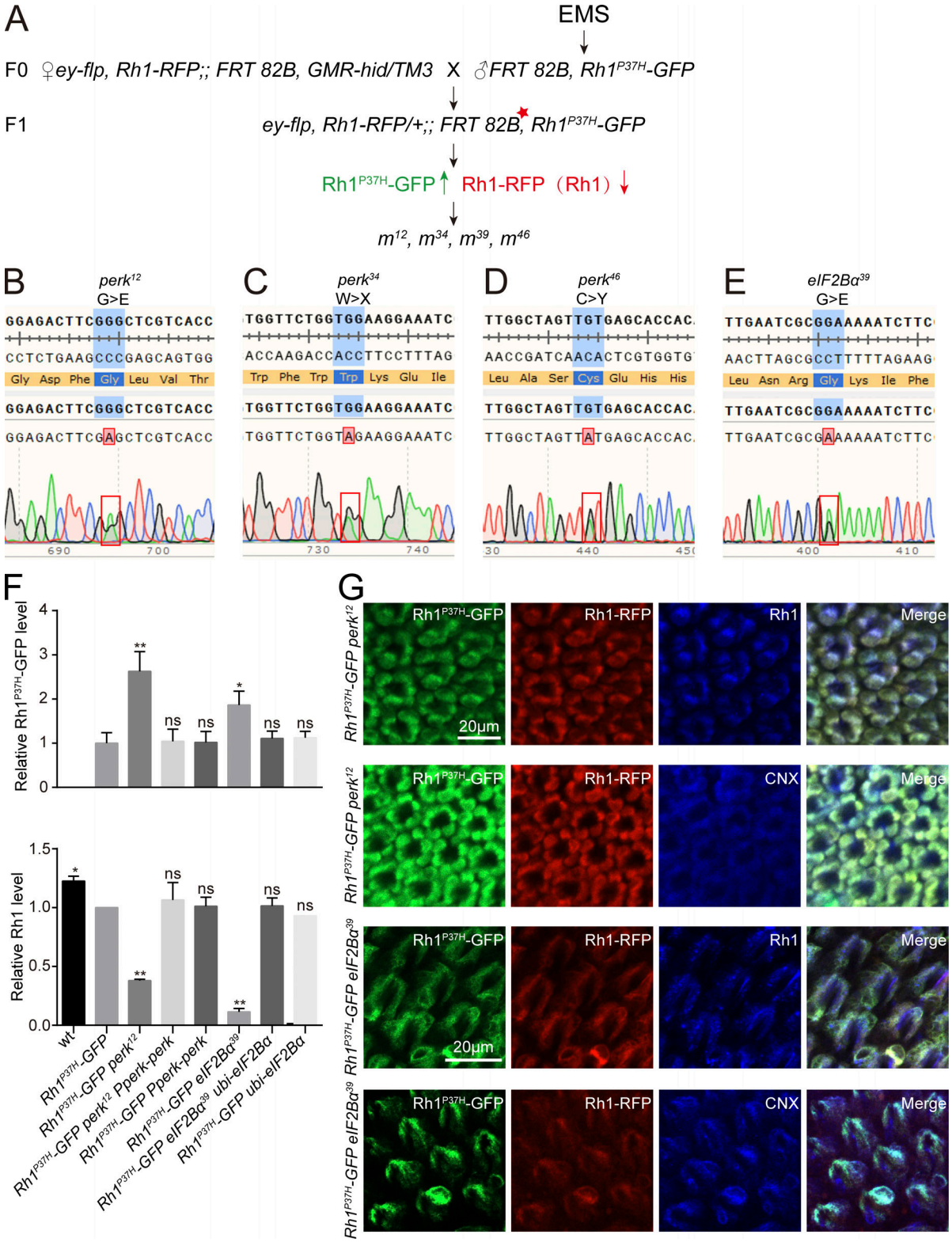

Figure S1. **Genetic screen reveals that *perk* and *eIF2Bα* are involved in Rh1 homeostasis in a model of adRP. (A)** EMS screening strategy to identify factors that regulate Rh1 homeostasis when Rh1^{P37H} is expressed. Screening the right arm of the third chromosome (3R) is used as an example. The *FRT82B Rh1^{P37H}-GFP* flies were isogenized, and male flies were fed 25 mM EMS (Sigma-Aldrich) in 2% sucrose for 8 h, followed by mating to *ey-flp Rh1-RFP; FRT82B GMR-hid CL/TM3* flies. Approximately 100,000 F1 progeny with homozygous mutant eyes were examined for fluorescence of GFP-tagged Rh1^{P37H} and RFP-tagged wild-type Rh1. **(B–E)** Mutations associated with the *perk^{12}*, *perk^{34}*, *perk^{46}*, and *eIF2Bα^{39}* alleles. **(F)** Quantification of protein levels of Rh1^{P37H}-GFP and endogenous Rh1 shown in Fig. 2 C. Error bars indicate SEM (n = 3); ns, not significant, *P < 0.1, **P < 0.01 (one-way ANOVA, Sidak's multiple comparisons test). **(G)** Staining *perk^{12}*, and *eIF2Bα^{39}* retina expressing Rh1^{P37H}-GFP and Rh1-RFP against CNX (blue, ER marker) and wild-type Rh1 (blue). GFP fluorescence of Rh1^{P37H}-GFP (green) and RFP fluorescence of Rh1-RFP (red) were directly observed. Scale bar, 20 μm.

https://doi.org/10.1083/jcb.202208147

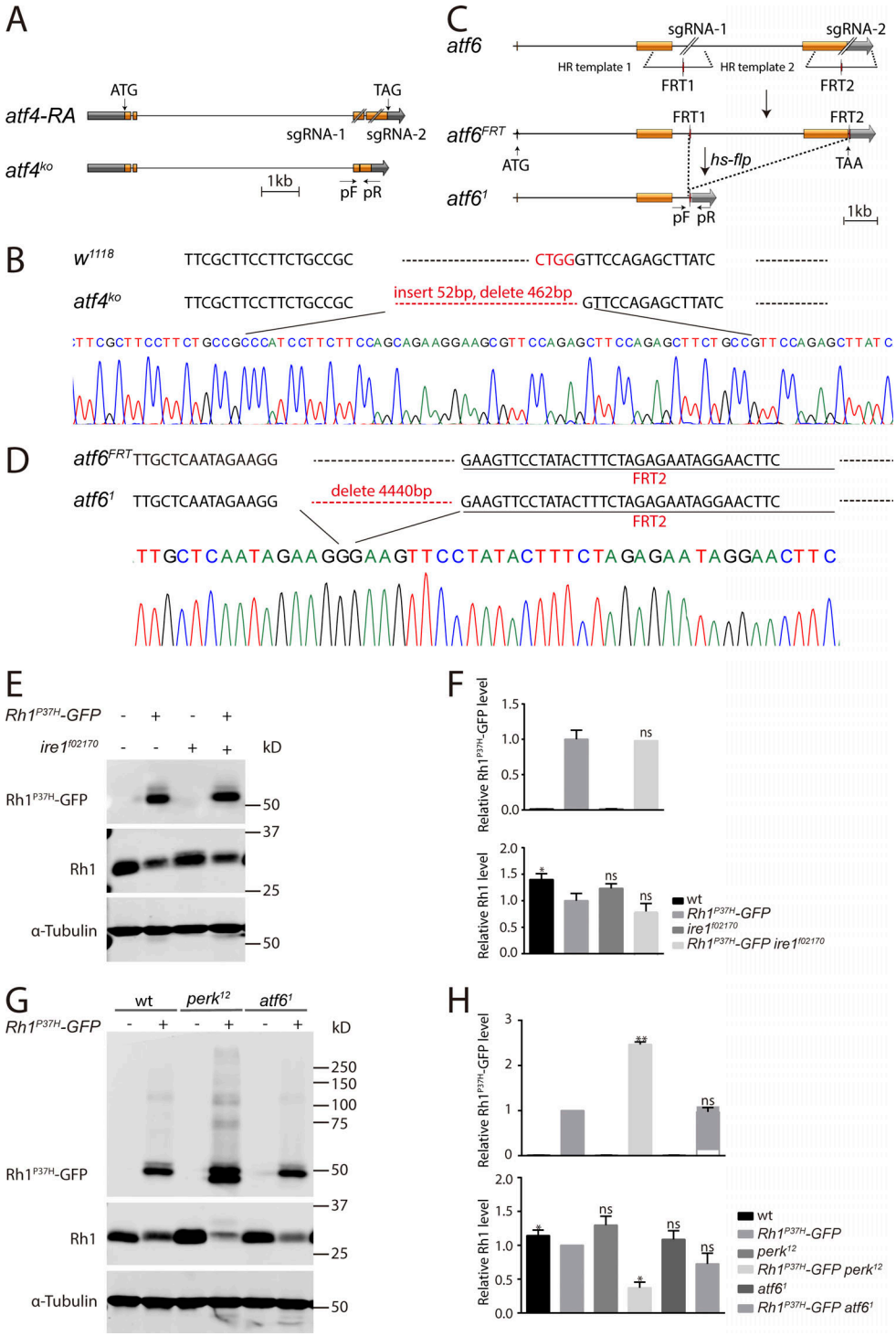

Figure S2. **Levels of Rh1^{P37H} and endogenous Rh1 were unaffected by mutations in the *ire1* and *atf6*. (A)** Schematic of *atf4* deletion through sgRNA targeting. Organization of the *atf4* locus and the expected structure of the deletion allele *atf4^{KO}* are shown. Orange boxes represent the coding region. The positions of the sgRNA pair and the DNA primers used for PCR (arrows, pF and pR) are indicated. **(B)** Verification of the *atf4^{KO}* locus by DNA sequencing. The *atf4^{KO}* mutation inserts 52 bp and eliminates 462 bp within the *atf4* locus. **(C)** Schematic of *atf6* deletion through sgRNA targeting and *Flp/FRT* recombination. Organization of the *atf6* locus and the structure of *atf6^{FRT}* and *atf6^{1}* is shown. Briefly, two *FRT* sites (red) were inserted into the *atf6* locus using CRISPR/Cas9-mediated homologous recombination. The *atf6^{FRT}* knock-in flies, were cross with *hs-flp* lines to delete the DNA fragments between the two *FRT* sites. PCR primers (arrows, pF and pR) were used to verify the *atf6^{1}* flies. **(D)** Verification of the *atf6^{1}* locus by DNA sequencing. The *atf6^{1}* mutation eliminates 4,440 bp within the *atf6* ^{FRT} locus. **(E and F)** Western blot of heads dissected from wild-type (*ey-flp Rh1-RFP; Rh1^{P37H}-GFP*) and *ire1* mutant (*ey-flp Rh1-RFP; FRT82B Rh1^{P37H}-GFP ire1^{f02170}/FRT82B GMR-hid CL*) flies against Rh1^{P37H}-GFP and Rh1 were shown (E) and quantified (F). Error bars indicate SEM (n = 3); ns, not significant, *P < 0.1 (one-way ANOVA, Sidak's multiple comparisons test). **(G and H)** Western blot analysis of Rh1^{P37H}-GFP and endogenous Rh1 in homozygous *atf6^{1}* (*atf6^{1}; Rh1^{P37H}-GFP*) null mutant heads. Error bars indicate SEM (n = 3); ns, not significant, *P < 0.1, **P < 0.01 (one-way ANOVA, Sidak's multiple comparisons test). Source data are available for this figure: SourceData FS2.

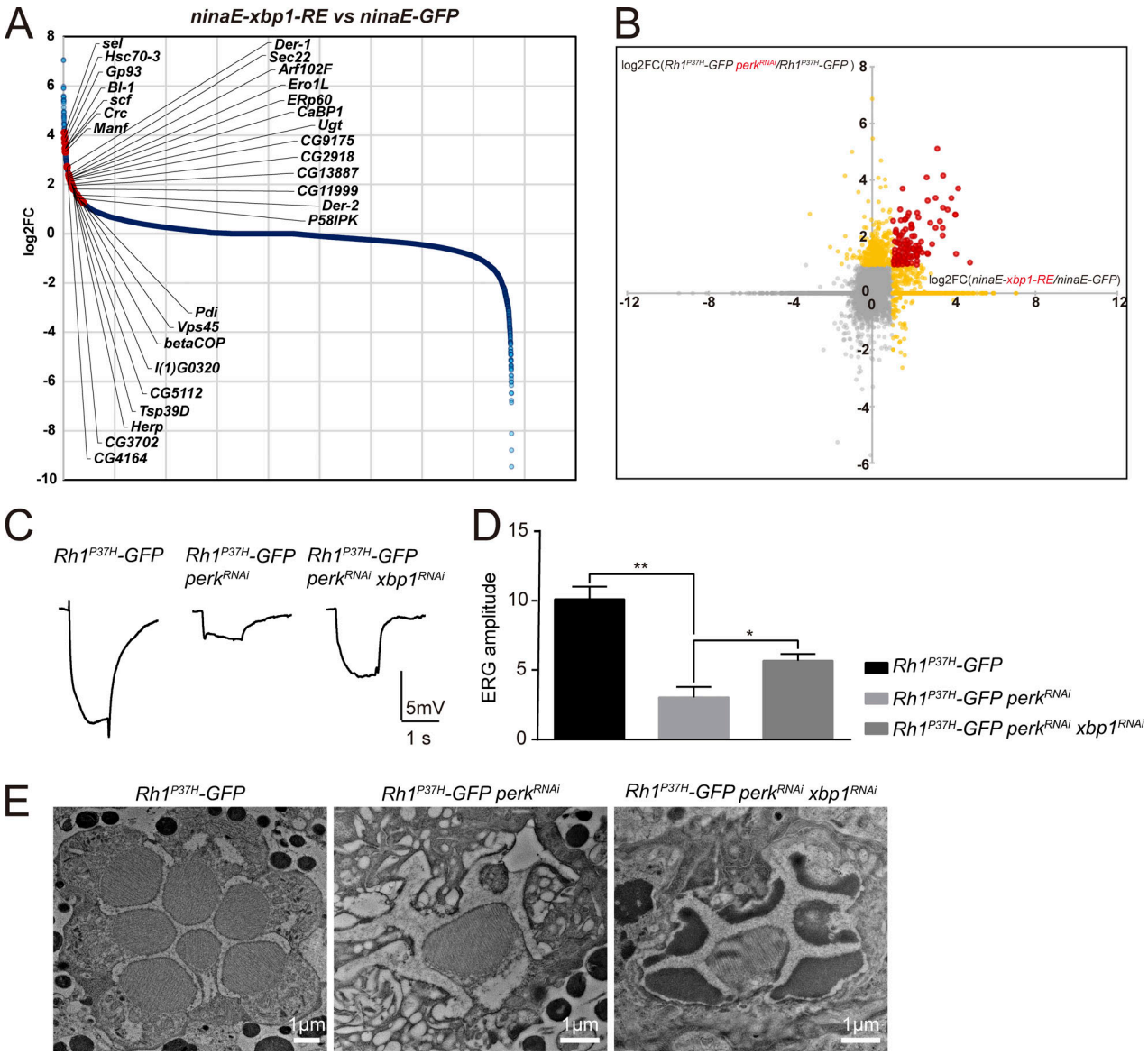

Figure S3. **Overlap of upregulated genes in *Rh1^{P37H}-GFP perk^{RNAi}* and *ninaE-xbp1-RE* retinas. (A)** Transcriptome profiling was used to compare gene expression between retina expressing XBP1-RE (*ninaE-xbp1-RE*) and GFP (*ninaE-GFP*) flies. Retinas were dissected from 1-d-old flies. Genes strongly upregulated by spliced XBP1 are indicated by red dots. **(B)** Analysis of upregulated genes in two RNA-seq experiments (*Rh1^{P37H}-GFP perk^{RNAi}* vs. *Rh1^{P37H}-GFP* and *ninaE-xbp1-RE* vs. *ninaE-GFP*). Genes upregulated in both *Rh1^{P37H}-GFP perk^{RNAi}* and *ninaE-xbp1-RE* flies are indicated by red dots. **(C and D)** ERG recordings show that expressing *xbp1^{RNAi}* restored visual responses in *Rh1^{P37H}-GFP perk^{RNAi}* flies. 5-d-old flies of indicated genotypes were exposed to a 1-s pulse of orange light after 2 min of dark adaptation. At least six flies were used for statistical analyses. Error bars indicate SEM (n = 6); *P < 0.1, **P < 0.01 (one-way ANOVA, Sidak's multiple comparisons test). **(E)** Representative TEM images of tangential sections through the eye of *Rh1^{P37H}-GFP perk^{RNAi}* flies that express *xbp1^{RNAi}* or not. Scale bar, 1 μm. Sectioned eyes were from 5-d-old flies.

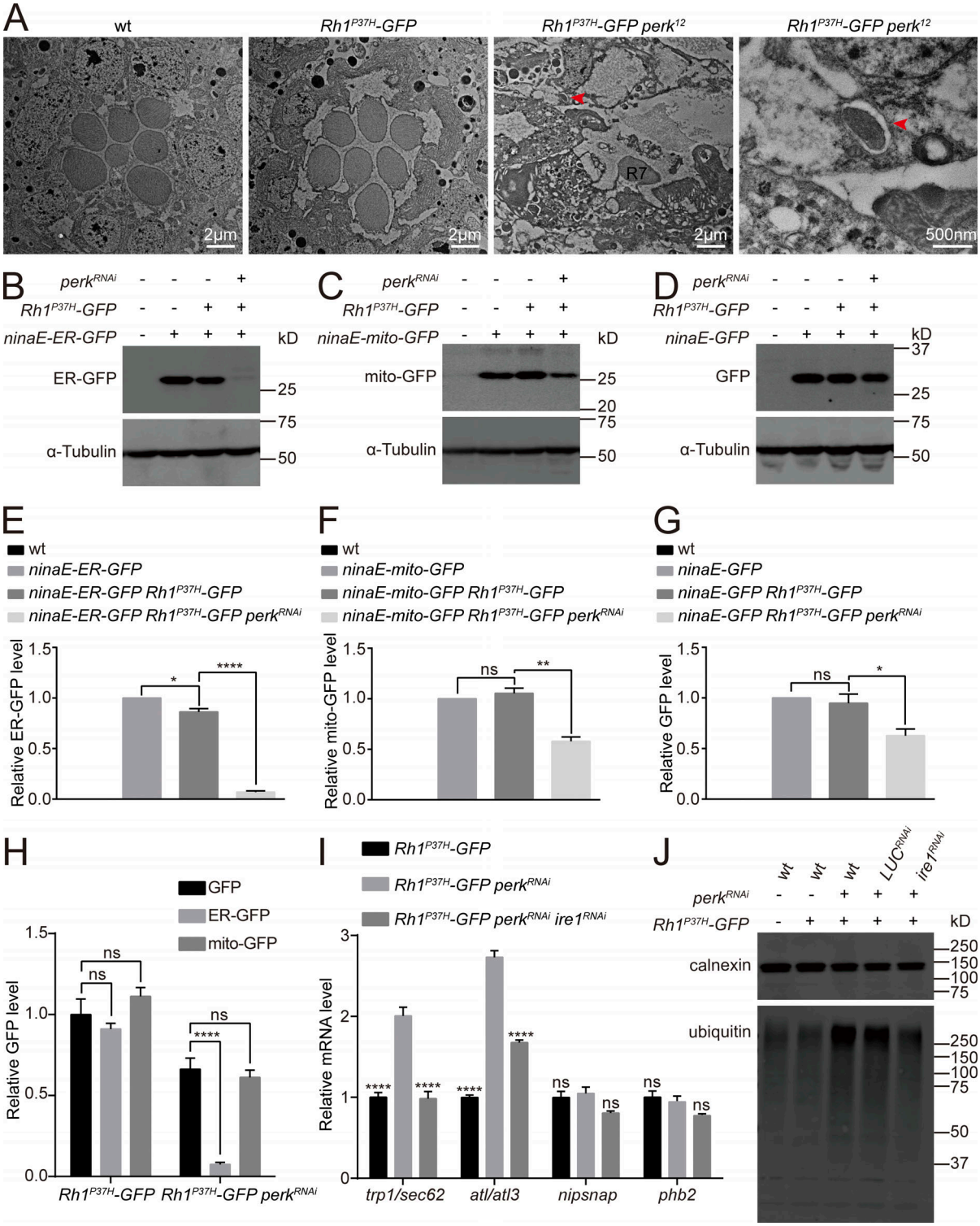

Figure S4. **ER proteins were degraded through autophagy in *Rh1^{P37H}-GFP perk^{RNAi}* photoreceptor cells. (A)** TEM images of tangential sections of compound eyes from 5-d-old wt (*w^{1118}*), *Rh1^{P37H}-GFP*, and *Rh1^{P37H}-GFP perk^{RNAi}* flies. Autophagosome are indicated by red arrows. Scale bars, 2 μm and 500 nm. All flies were in white eye background and raised under 12 h light/12 h dark cycles. **(B–H)** Western blotting against GFP to examine the effects of *perk^{RNAi}* on proteins with different subcellular localizations. ER-GFP was decreased in *Rh1^{P37H}-GFP perk^{RNAi}* flies, whereas *Rh1^{P37H}-GFP perk^{RNAi}* only slightly reduced mito-GFP and cytosolic GFP. Error bars indicate SEM (n = 6); ns, not significant, *P < 0.1, **P < 0.01, ****P < 0.0001 (one-way ANOVA, Sidak's multiple comparisons test). 1-d-old flies of indicated genotypes were used. **(I)** qPCR analysis showed that mRNAs encoding fly homologs of mammalian ER-phagy receptors (*trp1/sec62* and *atl/atl3*), but not homologs of mito-phagy receptors (*nipsnap* and *phb2*), were upregulated in the retina of *Rh1^{P37H}-GFP perk^{RNAi}* flies, compared with *Rh1^{P37H}-GFP* and *Rh1^{P37H}-GFP perk^{RNAi} ire1^{RNAi}* retina. Error bars indicate SEM (n = 3); ns, not significant, ****P < 0.0001 (two-way ANOVA, Sidak's multiple comparisons test). 1-d-old flies of indicated genotypes were used. **(J)** Accumulation of ubiquitinated proteins in membrane extracts of *Rh1^{P37H}-GFP perk^{RNAi}* flies. The membrane fraction was purified via centrifuge and labeled for ubiquitin and calnexin. Source data are available for this figure: SourceData FS4.

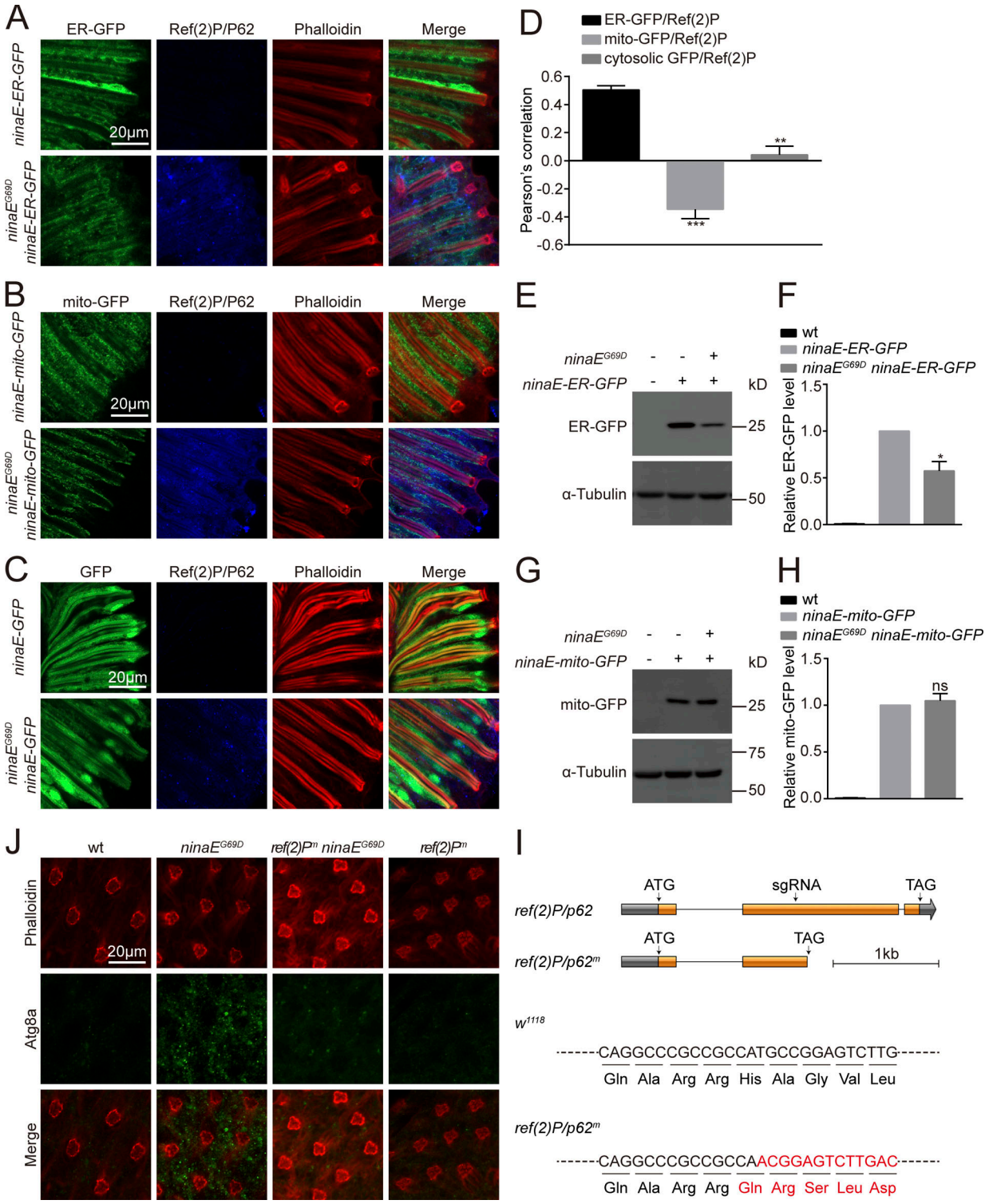

Figure S5. **ER-phagy was induced in the *ninaE*^{G69D} model of adRP. (A–D)** ER-GFP, but not mito-GFP or cytosolic GFP colocalized with Ref(2)P/P62 in *ninaE*^{G69D} photoreceptor cells. Longitudinal views of retinas from *ninaE-ER-GFP/ninaE*^{G69D} (A), *ninaE-mito-GFP/ninaE*^{G69D} (B), and *ninaE-GFP/ninaE*^{G69D}(C) flies labeled against GFP (green) and Ref(2)P/P62 (blue). Phalloidin (red) was used as a marker for rhabdomere. Scale bar, 20 μm. **(D)** Quantification of the co-localization between Ref(2)P/P62 and ER-GFP, mito-GFP, or cytosolic GFP in *ninaE*^{G69D} photoreceptor cells. Error bars indicate SEM (n = 3); **P < 0.01, ***P < 0.001 (Student's unpaired t test). **(E–H)** Western blotting against GFP to examine the levels of ER-GFP (E and F) and mito-GFP (G and H) in the *ninaE*^{G69D} background. Error bars indicate SEM (n = 3); ns, not significant, *P < 0.1 (one-way ANOVA, Sidak's multiple comparisons test). 1-d-old flies of indicated genotypes were used. **(I)** Generation of *ref(2)P*^{m} flies. Organization of the *ref(2)P/p62* locus is shown. A single sgRNA primer was used to generate the mutations. The *ref(2)P*^{m} frame-shift mutation was identified via DNA sequencing. **(J)** Immunostaining photoreceptor cells for Atg8a showed an increase in Atg8a puncta in *ninaE*^{G69D} photoreceptor cells. This was abolished when the *ref(2)P*^{m} mutation was introduced. Phalloidin served as a marker for ommatidia. Source data are available for this figure: SourceData FS5.

Provided online are Data S1, Data S2, and Data S3. Data S1 shows the gene expression profiling of retina of the *Rh1^{P37H}-GFP perk^{RNAi}* and *Rh1^{P37H}-GFP* flies related to Fig. 4 A. Data S2 shows the gene expression profiling of retina dissected from the *ninaE-GFP* and *ninaE-xbp1-RE* flies related to Fig. S3 A. Data S3 shows comparison of retinal protein levels of *Rh1^{P37H}-GFP perk^{RNAi}* with *Rh1^{P37H}-GFP* flies related to Fig. 5 A.